iScience

CellPress
OPEN ACCESS

Article

mNSCs overexpressing *Rimkla* transplantation facilitates cognitive recovery in a mouse model of traumatic brain injury

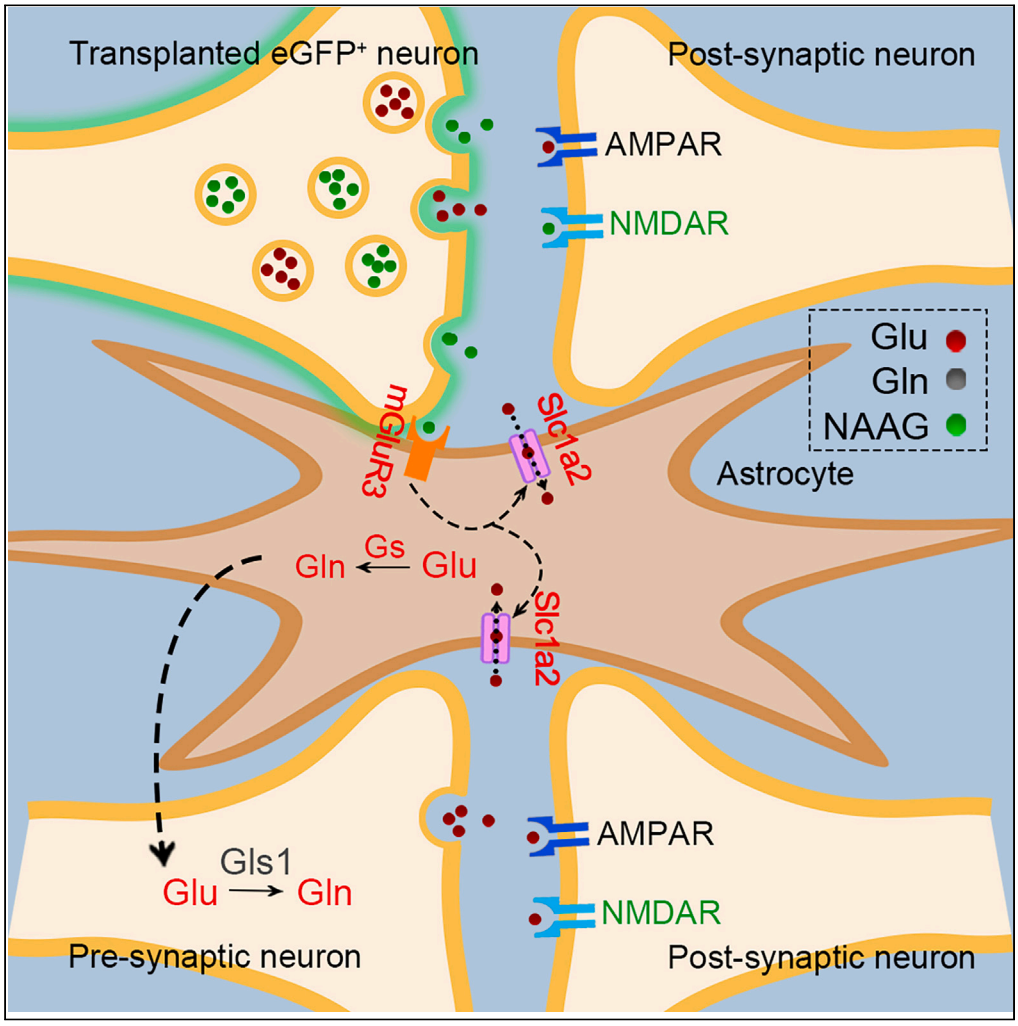

Tongjie Ji, Ying Pang, Meng Cheng, ..., Min Liu, Jing Zhang, Chunlong Zhong

rodger_lm@163.com (M.L.)
zhangjingwt@tongji.edu.cn (J.Z.)
drchunlongzhong@tongji.edu.cn (C.Z.)

Highlights

Rimkla knockout affected the differentiation of mNSCs

Grafted mNSCs overexpressing *Rimkla* promoted neuronal synaptic repair after TBI

Grafted mNSCs overexpressing *Rimkla* activated mGlur3 in astrocytes

Activated mGlur3 regulated neural glutamate-glutamine metabolism

Ji et al., iScience *26*, 107913
October 20, 2023
https://doi.org/10.1016/j.isci.2023.107913

iScience

CellPress
OPEN ACCESS

Article

mNSCs overexpressing *Rimkla* transplantation facilitates cognitive recovery in a mouse model of traumatic brain injury

Tongjie Ji,[1] Ying Pang,[1] Meng Cheng,[1] Rui Wang,[1] Xu Chen,[1] Chunyu Zhang,[1] Min Liu,[1,*] Jing Zhang,[1,2,*] and Chunlong Zhong[1,3,*]

SUMMARY

N-acetyl aspartyl-glutamate (NAAG) is easily inactivated for the hydrolysis of NAAG peptidase on the surface of glial cells, thereby losing its endogenous neuroprotective effect after traumatic brain injury. In this study, lentiviral vectors were used to over express/knock out NAAG synthetase II (*Rimkla*) in mouse embryonic neural stem cells (mNSCs) *in vitro* and these mNSCs were transplanted at the lesion site in a mouse model of controlled cortical impact (CCI). *In vivo* experiments showed that transplantation of mNSCs overexpressing *Rimkla* regulated glutamate-glutamine cycling between adjacent astrocytes and neurons in the subacute phase of CCI, thereby enhancing support for neuronal metabolism and promoting neuronal synaptic repair in the hippocampal CA3 region. Taken together, these findings demonstrate that transplantation of neural stem cells overexpressing *Rimkla* can effectively increase the NAAG concentration in local brain regions, which opens up new ideas for the maintenance of NAAG neuroprotective effects after TBI.

INTRODUCTION

Traumatic brain injury (TBI), which is complicated in cause, pathogenesis and clinical outcome, contributes to high mortality, disabled rates, and medical cost. There is a growing requirement to develop effective therapeutic interventions as the incidence of traumatic brain injury is further increasing for the development of modern means of transport.[1] Primary and secondary injury cascades are usually considered to be the two stages of TBI, while the latter stage plays an important role in pathophysiology of cerebral damage, including excitotoxic damage, inflammation, oxidative stress, and other pathological process.[2] Abundant researches have demonstrated that increased glutamate concentration in the synaptic cleft accompanied with pathological activation of N-methyl-D-aspartic acid receptors (NMDARs) facilitate excitotoxicity with a mechanism of intracellular calcium overload.[3]

N-acetyl aspartyl-glutamate (NAAG) is an N-acetylated dipeptide synthesized from N-acetyl-aspartate (NAA) and glutamate by NAAG synthetase II (*Rimkla*) in neurons. The neuromodulatory role of NAAG at glutamatergic synapses has been widely demonstrated.[4] NAAG can competitively bind to NMDARs in the postsynaptic membrane of neurons and block the excitotoxic effects of glutamate. It can also activate the metabotropic glutamate receptor 3 (mGlur3) on the presynaptic membrane of neurons and the surface of astrocytes, thereby inhibiting the excessive release of glutamate from the presynaptic neuron and regulating the glutamate transport from synaptic cleft to astrocytes.[5] Therefore, strategies of increasing NAAG concentration around the affected brain regions may be beneficial to counteract excessive glutamate signaling after TBI. However, NAAG released into the synaptic cleft is quickly hydrolyzed to NAA and glutamate by two zinc metallopeptidases, glutamate carboxypeptidase II (GCPII), and III (GCPIII) on the glial cell surface, thus losing its endogenous neuroprotective effect.[6] We previously demonstrated that treatment with NAAG peptidase inhibitor ZJ-43 significantly increased the concentration of NAAG in the dialysate of dorsal hippocampus in a rat fluid percussion injury (FPI) model and reduced acute neuronal degeneration and astrocyte damage, and this neuroprotective effect could be blocked by mGluR3 antagonist LY341495.[7,8] In addition, we demonstrated that GCPII knockout mice were less susceptible to traumatic brain injury with NAAG degradation inhibiting.[9] Nevertheless, we found that NAAG peptidase activity could not be completely inhibited in GCPII deficient mice. Hence more investigations are required to focus on maintaining the effective concentration of NAAG in the synaptic cleft after TBI.

Neural stem cells (NSCs) transplantation performed as promising strategies for treating traumatic brain injury. Many studies have shown that transplanted exogenous NSCs can survive for dozens of days in the host after TBI and exert long-term neuroprotective effect.[10] NSCs transplanted into the brain can migrate to the damaged brain tissue area, replace the damaged cells through further differentiation,

[1]Department of Neurosurgery, Shanghai East Hospital, School of Medicine, Tongji University, Shanghai, China
[2]Institute for Advanced Study, Tongji University, Shanghai, China
[3]Lead contact
*Correspondence: rodger_lm@163.com (M.L.), zhangjingwt@tongji.edu.cn (J.Z.), drchunlongzhong@tongji.edu.cn (C.Z.)
https://doi.org/10.1016/j.isci.2023.107913

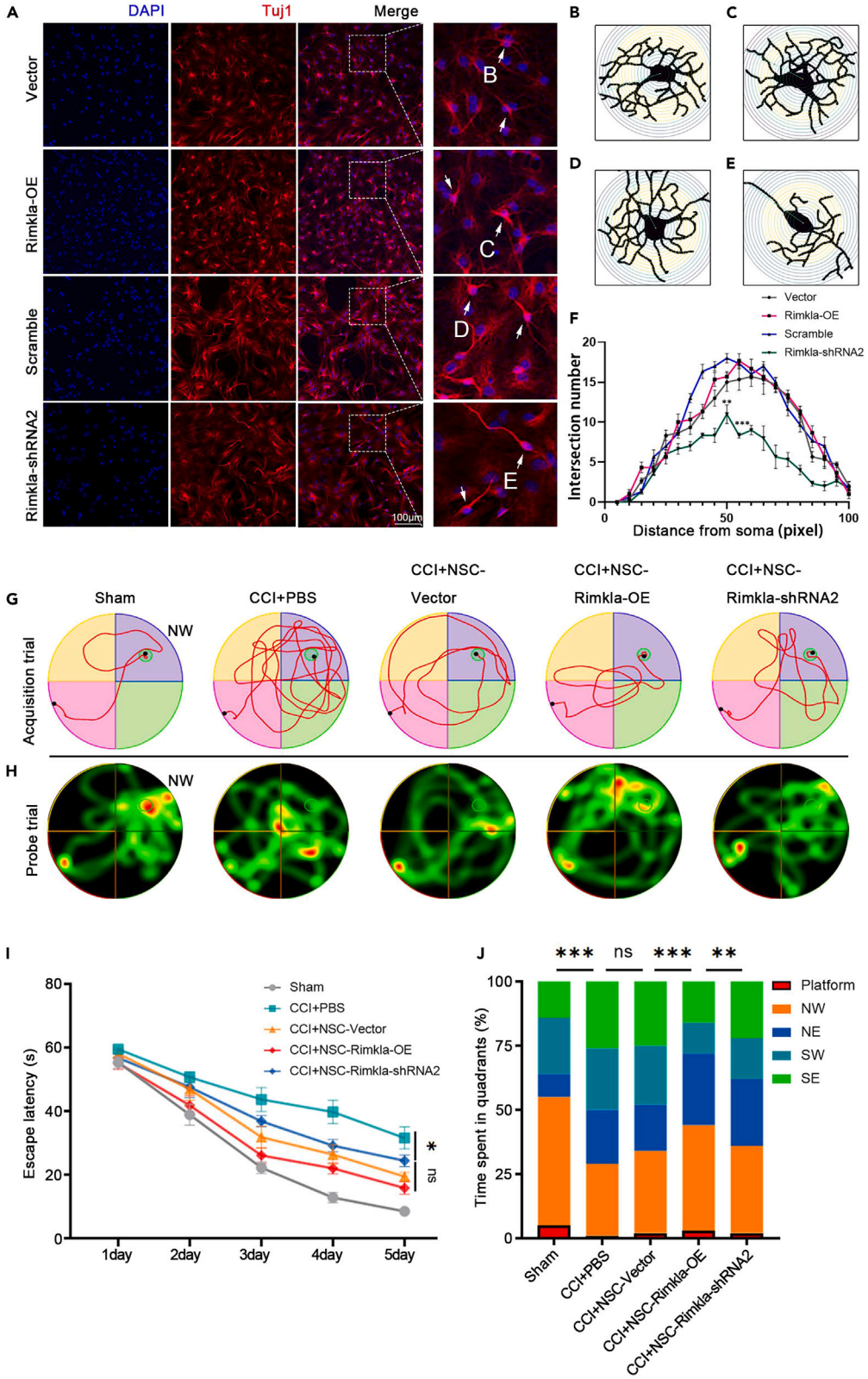
A
DAPI
Tuj1
Merge
Vector
Rimkla-OE
Scramble
Rimkla-shRNA2
B
C
D
E
100μm
B
C
D
E
F
Vector
Rimkla-OE
Scramble
Rimkla-shRNA2
Intersection number
Distance from soma (pixel)
G
Sham
CCI+PBS
CCI+NSC-Vector
CCI+NSC-Rimkla-OE
CCI+NSC-Rimkla-shRNA2
Acquisition trial
NW
H
Probe trial
NW
I
Sham
CCI+PBS
CCI+NSC-Vector
CCI+NSC-Rimkla-OE
CCI+NSC-Rimkla-shRNA2
Escape latency (s)
1day
2day
3day
4day
5day
*
ns
J
***
ns
***
**
Platform
NW
NE
SW
SE
Time spent in quadrants (%)
Sham
CCI+PBS
CCI+NSC-Vector
CCI+NSC-Rimkla-OE
CCI+NSC-Rimkla-shRNA2

Figure 1. Transplantation of mNSCs overexpressing *Rimkla* significantly facilitated the recovery of learning and memory impairment

(A) mNSCs were labeled with anti Tuj1 primary antibody (red) 10 days after induction of differentiation into neurons, nuclei labeled with DAPI (blue). Arrows indicate typical neuronal morphology.

(B–F) Sholl analysis of the typical neuronal synapses in each group (n = 3 per group).

(G) Morris water maze (MWM) test, mice in sham, CCI+PBS, CCI+NSC-Vector, CCI+NSC-*Rimkla*-OE, and CCI+NSC-*Rimkla*-shRNA2 groups (n = 12 per group) swam road maps on the last day of the place navigation test.

(H) Heatmap of swimming trajectory of mice in each group within 1min of probe test on the 6th day of MWM. The green circle in the NW quadrant represents the platform.

(I) Line plots record the average time taken by each group of mice to find the underwater platform from day 1 to day 5 in the place navigation test.

(J) The average proportion of time spent by mice in each group in the five regions of NW, NE, SW, SE and platform within 1 min of probe test was calculated. The error bars represent the S.E.M. NW northwest, NE northeast, SE southeast, SW southwest. *p < 0.05, **p < 0.01, ***p < 0.001.

participating in the repair of damaged brain tissue, and release growth factors and anti-inflammatory factors.[11] Considering the long-term neuroprotective effect of exogenous NSCs transplantation, we hypothesized that whether the transplantation of *Rimkla* modified NSCs could be used to more effectively maintain NAAG concentration in the synaptic gap after TBI, thereby prolonging its endogenous neuroprotective effect.

In this study, mild traumatic brain injury (mTBI) model was induced by controlled cortical impact (CCI) on mice.[12] 24 h after CCI, mouse embryonic neural stem cells (mNSCs) over expressing/knocking out *Rimkla* were transplanted into the lesion side of mouse hippocampus. *In vivo* experiments demonstrated that transplantation of mNSCs overexpressing *Rimkla* effectively increased the concentration of NAAG in the local brain area during the sub-acute phase of CCI, and then activated mGlur3 and Slc1a2 on the surface of astrocytes, thereby regulating glutamate-glutamine cycling between adjacent astrocytes and neurons. Furthermore, these changes enhanced metabolic support for neurons and promoted neuronal synaptic repair in the hippocampal CA3 region, and finally facilitated the recovery of learning and memory impairment. Taken together, our explorations open up new ideas for the maintenance of NAAG neuroprotective effects after TBI and provide a new strategy for the treatment of traumatic brain injury with NSC transplantation.

RESULTS

Transplantation of mNSCs overexpressing *Rimkla* significantly facilitated the recovery of learning and memory impairment

Primary mNSCs were isolated from P1-P3 mouse brains and grown as neurospheres. We measured the diameter of neurospheres from 0 days to 7 days and plotted the corresponding growth curves (Figures S1A and S1B). mNSCs were, respectively, cultured in the specific medium inducing differentiation into neurons, astrocytes, and oligodendrocytes for 10 days to verify its multi-directional differentiation potential. Immunofluorescence proved that the extracted mNSCs were successfully induced to differentiate into a variety of nerve cells (Figure S1C). Western blot confirmed the expression of Nestin, a kind of marker of NSCs, in the extracted mNSCs. (Figure S1D). mNSCs from different groups were collected for mRNA and protein detection 48 h after the last lentiviral infection, and the result of RT-qPCR and western blot demonstrated that we successfully constructed mNSCs over expressing or knocking down *Rimkla* (Figures S1D–S1F).

Tuj1 was used to label neurons differentiated from mNSCs to further explore the effect of *Rimkla* overexpression/knockdown on the development of mNSCs (Figure 1A). Sholl analysis showed that mNSCs overexpressing *Rimkla* normally differentiate into neurons *in vitro* (Figures 1B, 1C, and 1F), while *Rimkla* knockout resulted in synaptic development defects (Figures 1D–1F).

At 24 h after CCI, mice were divided into four groups and stereotaxically injected with PBS, NSC-Vector, NSC-*Rimkla*-OE, and NSC-*Rimkla*-shRNA2, respectively. The mice learning and memory was evaluated by morris water maze experiment 14 days after injection. On the last day of the place navigation test (the 5th day), the trajectory map of mice looking for the underwater platform (Figure 1G) showed that the average time for the NSC-Vector group mice to find the platform was significantly shorter than PBS group. There was no significant difference in the average time of finding platform between NSC-*Rimkla*-shRNA2 group and NSC-Vector group. Compared with the NSC-Vector group, the NSC-*Rimkla*-OE group took less time to find the platform, but it was still longer than the Sham group. Cumulative statistics of the time required for mice to find the platform in each group of 5-day place navigation test (Figure 1I) showed that PBS group mice were the slowest to find the platform, and the performance of mice in all mNSCs transplantation groups was better than the PBS group. Although the performance of NSC-*Rimkla*-OE group seemed better than NSC-Vector and NSC-*Rimkla*-shRNA2 groups, the difference was not statistically significant (Figure S1G). The heatmap of swimming trajectory of the mice in the probe test (Figure 1H) showed that the memory accuracy of the NSC-Vector group and NSC-*Rimkla*-shRNA2 group was better than PBS group, but worse than NSC-*Rimkla*-OE group. Quantitative analysis of the behavioral performance of mice in the place navigation test showed that the NSC-*Rimkla*-OE group mice had more times of crossing the original platform position and spent more time in the original platform quadrant (NW) than the NSC-Vector and NSC-*Rimkla*-shRNA group (Figures 1J, S1H, and S1I). The statistics of the mice average swimming speed in the place navigation test showed that the NSC-*Rimkla*-OE group mice swam faster than other two mNSCs injection groups, mice in all mNSCs injection groups swam significantly faster than the PBS group (Figure S1J).

These results indicated that transplantation of *Rimkla*-overexpressing mNSCs can facilitate the recovery of mouse learning and memory impairment after CCI, while transplantation of *Rimkla*-knockdown mNSCs significantly attenuated this trend. To further confirm the neuroprotective effect of *Rimkla*-overexpressing mNSCs, we then focused on the microscopic differences between NSC-Vector and NSC-*Rimkla*-OE groups.

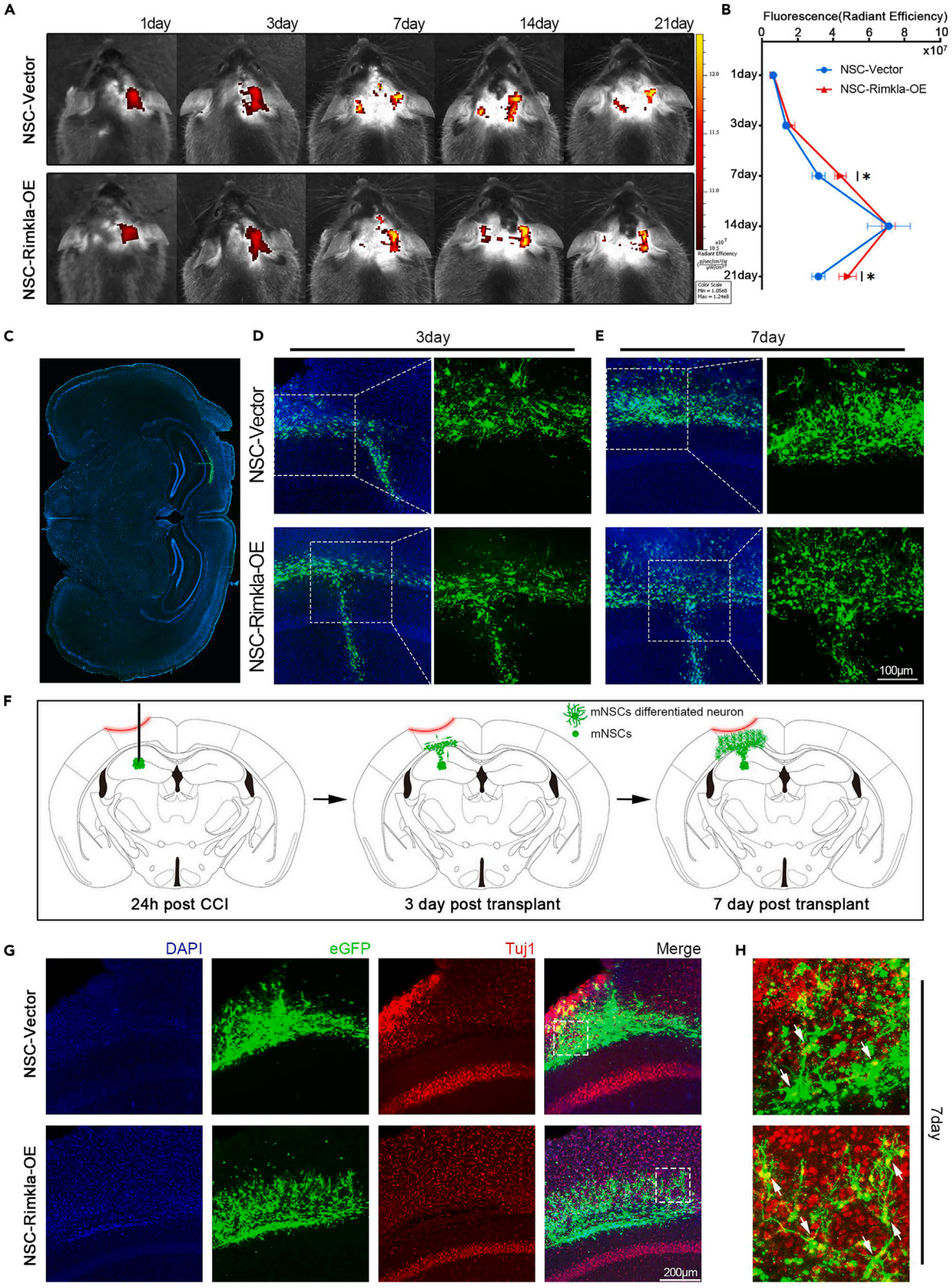
A
1day
3day
7day
14day
21day
NSC-Vector
NSC-Rimkla-OE
B
Fluorescence(Radiant Efficiency)
0 2 4 6 8 10
x10^7
NSC-Vector
NSC-Rimkla-OE
1day
3day
7day
14day
21day
C
D
3day
E
7day
NSC-Vector
NSC-Rimkla-OE
100μm
F
mNSCs differentiated neuron
mNSCs
24h post CCI
3 day post transplant
7 day post transplant
G
DAPI
eGFP
Tuj1
Merge
NSC-Vector
NSC-Rimkla-OE
200μm
H
7day

Figure 2. Overexpression of *Rimkla* affected the survival, migration, and differentiation of mNSCs *in vivo*

(A)Bioluminescence imaging results of transplanted mNSCs in TBI mice over 21 days.

(B) Quantification of bioluminescence imaging results of transplanted side (n = 5 per group).

(C) Coronal whole brain film scan at the mid-hippocampal level on day 3 after transplantation. eGFP (green) labeled transplanted mNSCs, and DAPI (blue) labeled nuclei.

(D and E) The migration and morphology of mNSCs in the hippocampus of mice in the Vector group and the *Rimkla*-OE group on the 3rd day and 7th day after transplantation. Scale bar, 100μm.

(F) Schematic representation of mNCSs migration and differentiation *in vivo* at 1, 3, and 7 days after transplantation.

(G and H) Anti-Tuj1 (red) primary antibody labeled neuronal cells and DAPI (blue) labeled nuclei on day 7 after mNSCs transplantation. Scale bar, 200μm. The right panel (H) is a magnified image after the merge of the fluorescence 488 and 555 channels, and the arrows indicate neurons with overlapping $eGFP^+$ and $Tuj1^+$ signals. The error bars represent the S.E.M. *$p < 0.05$.

Overexpression of *Rimkla* affected the survival, migration, and differentiation of mNSCs *in vivo*

Bioluminescence imaging *in vivo* was applied to determine the survival of grafted mNSCs 1day–21day post transplantation (Figure 2A). According to the statistical analysis of bioluminescence intensity at different time points (Figure 2B), on the whole, the fluorescence signal in the injured area of mice in two groups gradually increased from day 1 to day 14 until the peak, then the fluorescence signal gradually decreased after day 14, which reflected the status of transplanted mNSCs. However, the mean bioluminescence signal intensity of NSC-*Rimkla*-OE group was significantly higher than NSC-Vector group on day 7. Subsequently, the mean bioluminescence signal intensity of the two groups tended to be consistent on day 14 while the signal in NSC-Vector group decreased more significantly on the 21st day. To further clarify the proliferation, migration, and differentiation of mNSCs in two groups *in vivo*, eGFP fluorescence was observed by laser confocal scanning in the same coronal brain slices of different mNSCs injection groups. Figure (Figure 2C) shows the scan of overall brain slice on the 3rd day post mNSCs transplantation, which roughly reveals the injection site and migration of mNSCs. The brain slices of mice showed that the $eGFP^+$ signal area was larger on the 7th day than the 3rd day after transplantation in both groups, and $eGFP^+$ cells had more obvious synaptic morphology on the 7th day (Figure 2D). There was no significant difference in the eGFP fluorescence signal area between the NSC-Vector group and the NSC-*Rimkla*-OE group at 3rd day post transplantation (Figures 2E and S2A). Besides, there was also no statistically significant difference in the distance between the widest points on both sides of the "T" shape of the eGFP signal (Figure S2B). However, the eGFP fluorescence area in NSC-*Rimkla*-OE group was significantly larger than NSC-Vector group at 7th days (Figures 2E and S2A). And the distance between the widest points on both sides of the "T" -shaped eGFP signal in the NSC-*Rimkla*-OE group was also significantly larger than the NSC-Vector group (Figure S2B). The migration, differentiation, and morphology of mNSCs *in vivo* was simulated according to the eGFP signal at different time points (Figure 2F). To explore whether there were neurons in $eGFP^+$ cells on 7th day after transplantation, we labeled neurons in brain slices with Tuj1 and found that some cells expressed both Tuj1 and eGFP signals. This indicated that part of the transplanted mNSCs differentiated into neurons (Figures 2G and 2H). Quantitative analysis of Tuj1 and eGFP fluorescence signals showed that the proportion of mNSCs differentiated into neurons in the NSC-*Rimkla*-OE group was significantly increased *in vivo* (Figure S2C).

mNSCs transplantation decreased astrogliosis and neuronal loss in the hippocampus

To further explore the unique neuroprotective effect of NSC-*Rimkla*-OE (abbreviated as NSC-*Rimkla*), changes in the protein expression of neuron, astrocyte, and microglia markers were examined in the lesion side of hippocampus in each group on the 3rd and 7th day after transplantation. Gfap and Iba1 in all injury groups were significantly higher than the Sham group on the 3rd day, but there was no significant difference among all the injury groups. Tuj1 expression was decreased in all injury groups, and there was no significant difference between all injury groups either (Figures S2D and S2E). Interestingly, the expression of these cell markers began to differ significantly between mNSCs injection groups on the 7th day post transplantation. The expression of these cell markers in Sham group was statistically different from all injury groups. The Gfap expression in NSC-Vector group and NSC-*Rimkla* group was significantly lower than PBS group, while Tuj1 in these two groups was higher than PBS group, but there was no significant difference between NSC-vector group and NSC-*Rimkla* group. The expression of microglia marker Iba1 in NSC-Vector group was higher than PBS group and NSC-*Rimkla* group (Figures 3A and 3B). RT-qPCR confirmed the consistent trend at mRNA level (Figures 3C and 3D). Immunohistochemistry (Figures 3E, 3G, S2F, and S2G) further verified the statistical differences in the number of astrocytes and microglia in the hippocampal CA3 region of mice in each group. Nissl staining also demonstrated that grafted mNSCs could effectively decrease neuronal loss in the hippocampal CA3 region of mice on 7th day after transplantation (Figure 3F). Finally, immunofluorescence was used to simultaneously label Tuj1 and Gfap to more clearly show the relationship between the number and location of neurons and astrocytes in the hippocampal CA3 region (Figures 3I–3K). It was observed that on the 7th day after transplantation, the density of neurons in the hippocampal CA3 region in the PBS group significantly decreased, the cells were loosely arranged, and more scattered neurons were seen (Figure 3I). Although there was no significant difference in the number of neurons in the hippocampus between the NSC-Vector and NSC-*Rimkla* groups, we unexpectedly found that NSC-*Rimkla* improved synaptic repair in the hippocampal neurons on the 7th day after transplantation (Figures 3A and S2D). Therefore, we focused on the synaptic morphology and synapse-associated protein in the hippocampal CA3 region of the lesion side in each group.

Transplantation of mNSCs overexpressing *Rimkla* promoted neuronal synaptic repair

Map2 was used to mark the synapses in the CA3 region of hippocampus on the lesion side. The synapses of CA3 neurons in the Sham group were complete and clear with good morphology while synapses in PBS group and NSC-Vector group became thinner and discontinuous.

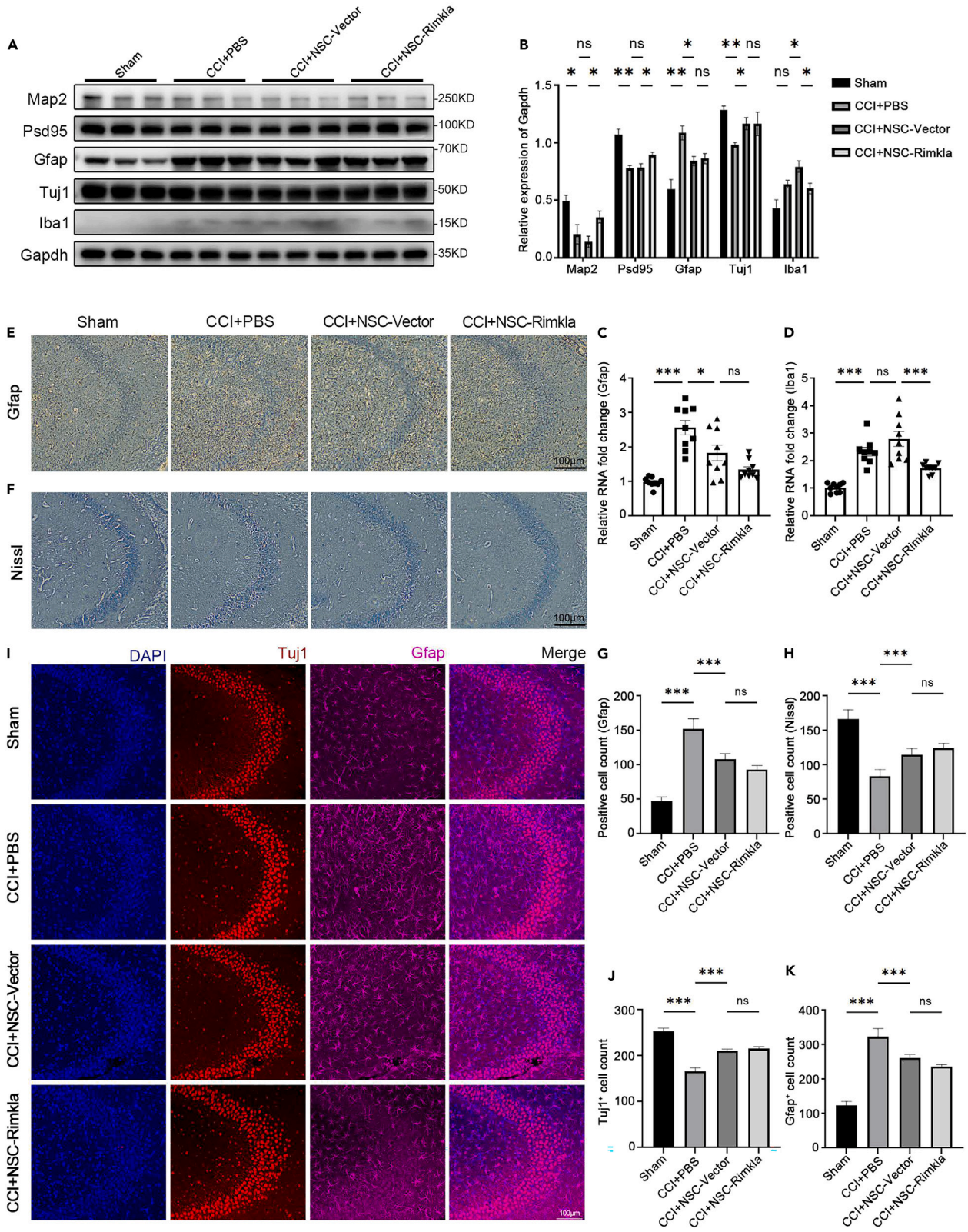
A
Sham
CCI+PBS
CCI+NSC-Vector
CCI+NSC-Rimkla
Map2
Psd95
Gfap
Tuj1
Iba1
Gapdh
250KD
100KD
70KD
50KD
15KD
35KD
B
Relative expression of Gapdh
Map2
Psd95
Gfap
Tuj1
Iba1
C
Relative RNA fold change (Gfap)
D
Relative RNA fold change (Iba1)
E
Gfap
F
Nissl
100μm
G
Positive cell count (Gfap)
H
Positive cell count (Nissl)
I
DAPI
Tuj1
Gfap
Merge
J
Tuj1+ cell count
K
Gfap+ cell count

Figure 3. mNSCs transplantation decreased astrogliosis and neuronal loss in the hippocampus

(A and B) The protein levels of Map2, Psd95, Gfap, Tuj1, and Iba1 in the hippocampus of mice in the Sham, CCI+PBS, CCI+NSC-Vector, and CCI+NSC-*Rimkla* groups were detected by western blot on day 7 after transplantation. (n = 3 per group). The right panel (b) is a quantitative analysis of the gray value and area of the immunoblot bands.

(C and D) RT-qPCR was used to detect the mRNA expression of Gfap and Iba1 in the hippocampus of mice in the previous groups (n = 9 per group).

(E) Immunohistochemistry and primary anti-GFAP antibody were used to label astrocytes in the hippocampal CA3 region of the transplanted side of mice in the above groups. Scale bar, 100μm (F) Nissl staining was used to label the neurons in the CA3 region of the hippocampus on the transplanted side of mice in each group. Scale bar, 100μm.

(G) Number of astrocytes in hippocampal CA3 region in immunohistochemistry. (n = 5 per group).

(H) Number of neurons in hippocampal CA3 region in Nissl staining. (n = 5 per group).

(I) Immunofluorescence staining of neurons and astrocytes in the CA3 region of the hippocampus on the 7th day after transplantation in each group. DAPI (blue) labeled nuclei, Tuj1 (red) labeled neurons, and Gfap (purple) labeled astrocytes. Scale bar, 100μm.

(J and K) Tuj1-positive and GFAP-positive cells were counted on immunofluorescence images (n = 5 per group). The error bars represent the S.E.M. *$p < 0.05$, **$p < 0.01$, ***$p < 0.001$.

However, the synapses in the NSC-*Rimkla*-OE group (abbreviated as NSC-*Rimkla*) recovered to some extent in morphology (Figure 4A). The measurement of synaptic diameter in hippocampal CA3 at the same location (dotted white line) showed that the average synaptic diameter in NSC-*Rimkla* group was significantly higher than the PBS group and NSC-Vector group, but still lower than the Sham group (Figures 4A and 4B). To further explore the effects of grafted mNSCs on synaptic repair after CCI, some typical synapse-associated genes were measured by RT-qPCR. Similarly, mRNA levels of Map2 and Psd95 showed a consistent trend with the morphological changes (Figures 4C and 4D). However, the expression of Syn and Gap43 showed no statistical difference not only within all mNSCs injection groups, but also between the PBS group and the Sham group (Figures S2H and S2I). It is worth noting that the expression of Camk2a was significantly decreased after CCI, but the injection of NSC-*Rimkla* helped to rescue this decline, though there was no significant difference in the expression of Camk2b between the groups (Figures 4E and S2J). We then investigated whether grafted NSC-*Rimkla* had any effect on neuronal dendritic spines by Golgi staining. Neurons in the hippocampal CA3 region were selected for observation, and the synaptic density in all mNSCs transplantation groups was greater than the PBS group (Figure 4F). Sholl analysis of neuronal synapses in the CA3 region of different groups showed that the PBS group had the lowest synaptic density, and the NSC-*Rimkla* group had slightly higher synaptic density than the NSC-Vector group, but the difference was not statistically significant (Figure 4G). The density of dendritic spines in the PBS group and NSC-Vector group was significantly reduced, while that in the NSC-*Rimkla* group was increased (Figures 4F and 4H). Further analysis of dendritic spine morphology showed that the proportion of mushroom-like dendritic spines in the NSC-*Rimkla* group was significantly higher than the PBS and NSC-*Rimkla* groups (Figures 4F and 4I).

Grafted mNSCs overexpressing *Rimkla* activated glutamate metabolism related pathways

In order to clarify the mechanism by which grafted NSC-*Rimkla*-OE (abbreviated as NSC-*Rimkla*) promotes synaptic repair of hippocampal neurons after TBI, we took the hippocampus on the lesion side of NSC-Vector and NSC-*Rimkla* groups on the 7th day after transplantation for whole transcriptome sequencing. After dimensionality reduction and clustering of sequencing results, it was found that the overall mRNA expression of hippocampus differed between NSC-Vector and NSC-*Rimkla* groups (Figures 5A and S3A). 3286 differential genes were screened out after differential gene analysis (Figures 6B and S3B) and "glutamine family amino acid biosynthetic process", "L-glutamate import across plasma membrane", "channel regulator activity", "synaptic repair", "learning and memory" related pathways were enriched after GO analysis, which further confirmed the neuroprotective effect of grafted NSC-*Rimkla* (Figure 5C). Furthermore, the hippocampal glutamate transporters and receptors (including Slc1a2, Gls, mGlur3) and synaptic repair related genes (including Ngfr, Syt4, Npas4) were found to be significantly higher in the NSC-*Rimkla* group than NSC-Vector group (Figure 5D). The total concentrations of glutamate, NAAG, γ-aminobutyric acid (GABA), and NAA in the hippocampus on the 3rd and 7th day after transplantation were measured by LC-MS/MS. On the 3rd day, contents of NAAG and NAA in NSC-*Rimkla* group were significantly higher than PBS group and NSC-Vector group (Figures 5E and S3C). However, there was no significant difference in glutamate, GABA, and Glu/GABA among all the CCI groups, and all CCI groups were significantly lower than the Sham group (Figures 5F–5H). Contents of NAAG and NAA in NSC-*Rimkla* group significantly increased on the 7th day while these in the PBS and NSC-Vector groups were still slightly lower than the Sham group (Figures 5I and S3D). This was accompanied by a remarkable increase of glutamate, GABA, and Glu/GABA in NSC-*Rimkla* group (Figures 5J–5L).

mGlur3 and Slc1a2 on the surface of astrocytes were activated near eGFP$^+$ synaptic terminals

Based on the results of whole transcriptome sequencing, some genes of interest in the hippocampus of lesion side on the 7th day after CCI was verified by RT-qPCR. The expressions of mGlur3, Slc1a2, and Glutaminase in NSC-Rimka-OE group (abbreviated as NSC-*Rimkla*) were significantly higher than the other three groups (Figures 6A–6C). Slc1a3 expression in all CCI groups was lower than Sham group, but there was no significant difference among CCI groups (Figure S3E). In addition, The NMDA receptor subunits NR2a and NR2b in NSC-*Rimkla* group were not significantly lower than other CCI groups (Figures 6D and S3F). Previous studies have demonstrated that activation of mGlur3 receptors on the surface of astrocytes activates the glutamate transporter Slc1a2 on astrocytes. Therefore, we focused on exploring the spatio-temporal expression of mGlur3 and Slc1a2 in the hippocampus of NSC-Vector and NSC-*Rimkla* groups after transplantation. Western blot confirmed that there was no statistically significant difference in the expression of mGlur3 and Slc1a2 in the hippocampus among all CCI

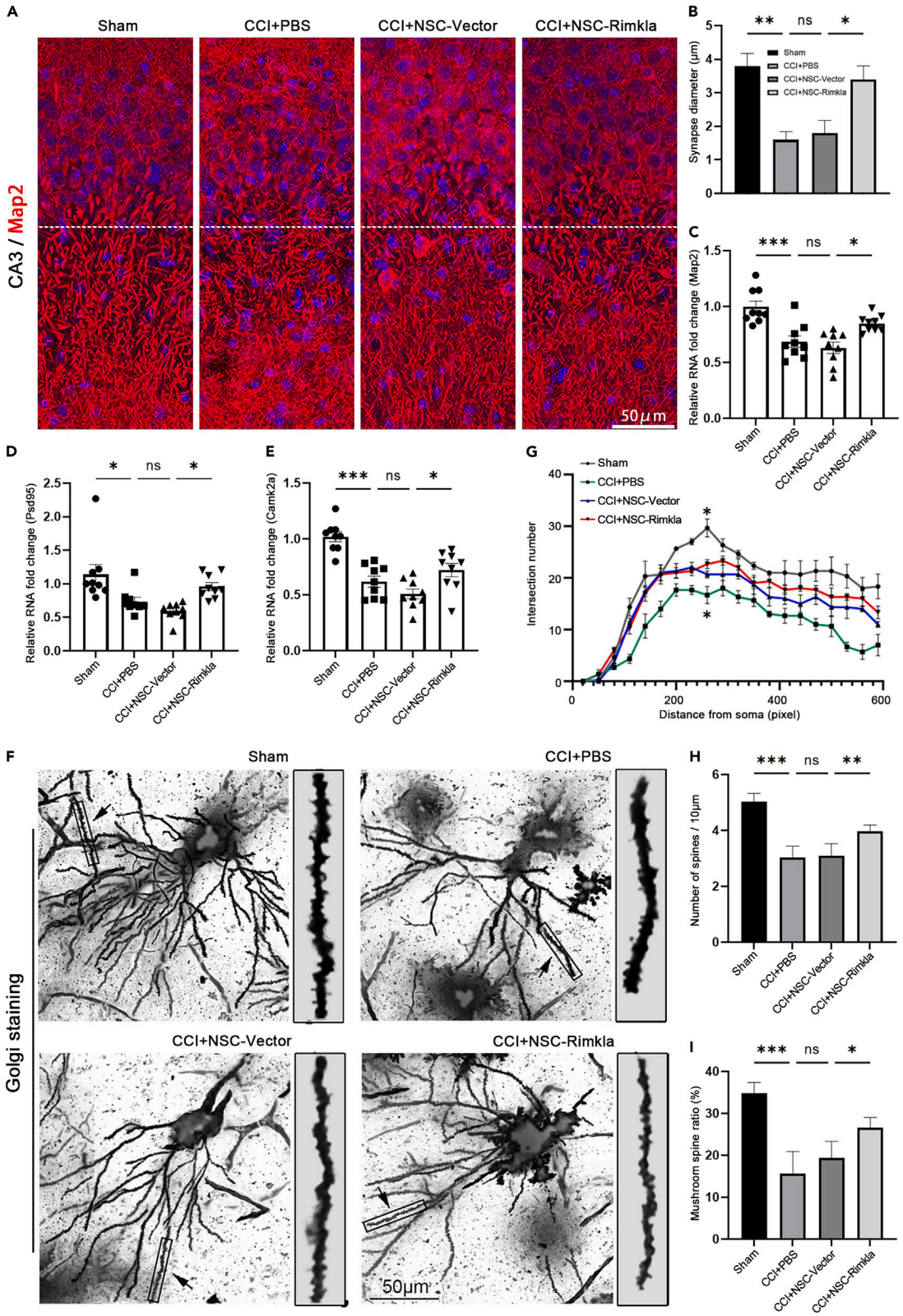
A
Sham
CCI+PBS
CCI+NSC-Vector
CCI+NSC-Rimkla
CA3 / Map2
50μm
B
Synapse diameter (μm)
C
Relative RNA fold change (Map2)
D
Relative RNA fold change (Psd95)
E
Relative RNA fold change (Camk2a)
G
Intersection number
Distance from soma (pixel)
F
Golgi staining
50μm
H
Number of spines / 10μm
I
Mushroom spine ratio (%)

Figure 4. Transplantation of mNSCs overexpressing *Rimkla* promoted neuronal synaptic repair

(A and B) Primary anti-Map2 antibody and immunofluorescence staining were used to mark neuronal synapses in the hippocampal CA3 region of the injured side on the 7th day after transplantation. Scale bar = 50μm. Right panel (B) measured dashed plane synaptic diameters (n = 5 per group).

(C–E) RT-qPCR was used to detect the mRNA expression of Map2, Psd95 and Camk2a in the injured hippocampus of mice (n = 9 per group).

(F) Golgi staining, hippocampal CA3 neurons in the injured hippocampus of mice. Scale bar, 50μm. Typical synapses were intercepted and displayed in magnification.

(G) Sholl analysis of synapses in Golgi-stained hippocampal CA3 region neurons (n = 3 per group).

(H) Analysis of dendritic spine density of neurons in each Golgi staining group (n = 5 per group).

(I) Statistical analysis of the proportion of mushroom dendritic spines in total dendritic spines of neurons in each group (n = 5 per group). The error bars represent the S.E.M. *p < 0.05, **p < 0.01, ***p < 0.001.

groups on the 3rd day (Figures S3G and S3H). However, the expressions of mGlur3 and Slc1a2 in NSC-*Rimkla* group were significantly increased on the 7th day (Figures 6E and 6F). To further figure out the reasons for this change, we labeled mGlur3 and Slc1a2 on the brain slices of the mice on the 7th day after transplantation by immunofluorescence and found that the expression of mGlur3 and Slc1a2 in the cells near the eGFP$^+$ synaptic terminals in the NSC-*Rimkla* group was significantly increased while this change was not observed in the NSC-Vector group (Figure 6G). Black arrows indicate cells with significantly high expression of mGlur3 and Slc1a2. In addition, the expression of mGlur3 and Slc1a2 in the hippocampal CA3 region in the subacute phase of CCI was significantly decreased, and the grafted mNSCs overexpressing *Rimkla* could significantly reverse this decline (Figures S3I–S3K).

DISCUSSION

This study aims to explore whether the transplantation of mNSCs overexpressing the NAAG synthetase II (*Rimkla*) after TBI can increase the local concentration of NAAG in the brain tissue, thereby prolonging the neuroprotective effect of NAAG in the acute/subacute phase after TBI. We found that transplantation of mNSCs overexpressing *Rimkla* after CCI more effectively facilitated the recovery of learning and memory impairment. Subsequently, multi-omics studies revealed that grafted mNSCs overexpressing *Rimkla* enhanced support for neuronal metabolism and promoted neuronal synaptic repair in the hippocampal CA3 region by regulating glutamate-glutamine cycling between adjacent astrocytes and neurons in the subacute phase of CCI.

We successfully constructed *Rimkla* overexpress/knockdown mNSCs (NSC-*Rimkla*-OE, NSC-*Rimkla*-shRNA2) with lentiviral vectors and demonstrated that *Rimkla* overexpression had no effect on mNSCs development. In order to study the effect of grafted mNSCs on the hippocampal after CCI, mouse learning and memory were evaluated 14 days after transplantation by morris water maze.[13] In place navigation test, the learning curve of mice in NSC-*Rimkla*-OE group was not significantly better than other mNSCs injection groups, and all mNSCs injection groups performed better than PBS group. But mice with NSC-*Rimkla*-OE showed more accurate memory of the platform location in probe test. It has been confirmed in many disease models that NSCs transplantation enhances cognition or learning and memory in mice or rats.[11,14,15] Besides, many studies have demonstrated that grafted NSCs plays a neuroprotective role in animal brain trauma models.[16–18] Here our investigation confirmed that mNSCs transplantation effectively promoted the recovery of mouse learning and memory, which was highly consistent with the previous researches. On this basis, mice in NSC-*Rimkla*-OE group showed further improvement in learning and memory compared with NSC-Vector group, suggesting that transplantation of mNSCs overexpressing *Rimkla* has a unique neuroprotective effect.

Studies have reported that exogenous NSCs transplanted *in vitro* undergo a three-phase change in the host, including post-transplantation apoptotic phase (1–3 days), proliferation and migration phase (3–14 days), and post-apoptotic phase (14 days).[10] The fate of *Rimkla*-overexpressing mNSCs transplanted in the hippocampus is still unknown. Bioluminescence imaging (Figure 2) showed that the bioluminescence intensity of mNSCs in the *Rimkla* and Vector groups on the 3rd day was not significantly weakened compared with the 1st day after transplantation. The following reasons may explain this phenomenon. First, in this experiment, mNSCs were transplanted in the hippocampal DG area of mice rather than the lateral ventricle, which might lead to different fate of grafted NSCs. Second, reduced tissue shading due to cell migration to the cortical surface counteracts the effect of cell death. Third, eGFP fluorescent protein does not degrade immediately after cell death. Interestingly, the bioluminescence intensity of the NSC-*Rimkla*-OE group was higher than the NSC-Vector group during both the proliferation and migration phase (7 days) and the post-apoptotic phase (21 days). One or more of the following reasons may contribute to this result. Overexpression of *Rimkla* might (1) improve mNSCs proliferation *in vivo*, (2) improve the ability of mNSCs to migrate to the cortex *in vivo*, (3) reduce mNSCs apoptosis after transplantation. To further clarify the reason for this change, coronal brain slices from the mNSCs transplantation site was obtained on the 3rd and 7th day post transplantation by shaking sectioning, which clearly demonstrated the migration and differentiation of mNSCs *in vivo*. The migration distance and area of *Rimkla*-overexpressing mNSCs were significantly higher than normal mNSCs on the 7th day, while the number of eGFP$^+$ cells was not significantly different between the two groups. Fluorescence staining of neuronal marker Tuj1 and eGFP fluorescence indicated that NSC-*Rimkla*-OE had a higher proportion of differentiating into neurons *in vivo*. These phenomena indicated that mNSCs overexpressing *Rimkla* had a significantly enhanced ability to migrate and differentiate into neurons *in vivo*.

Although there were differences in migration and differentiation of mNSCs between different genotype groups *in vivo*, it was not sufficient to explain the neuroprotective effect of NSC-*Rimkla*. To further clarify the occurrence time and microscopic mechanism of this neuroprotective effect, we focused on the changes of some major nerve cells in the hippocampus, especially the hippocampal CA3 region which is more sensitive to TBI.[19] Studies have reported that a large number of pyramidal neurons in the CA3 region apoptosis and inflammatory cells such as microglia are activated in the TBI acute phase (0–24 h) and subacute phase (1–7 days) accompanied by astrogliosis. The death of neurons and

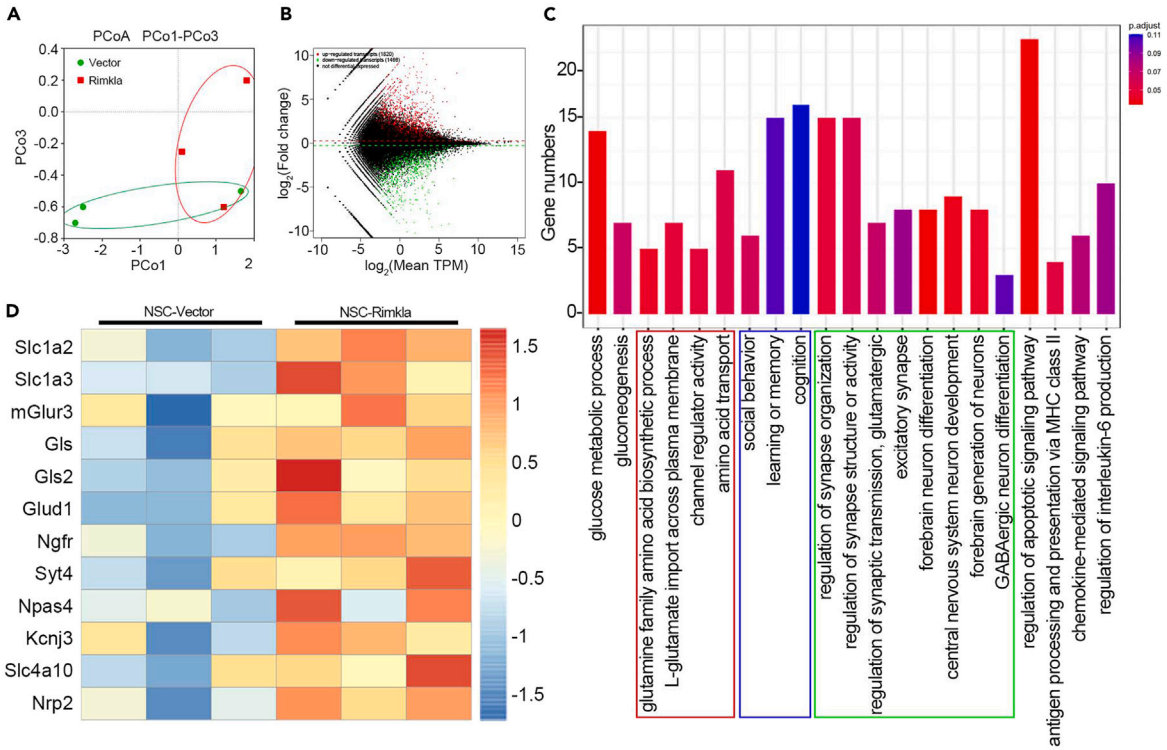
A
PCoA PCo1-PCo3
Vector
Rimkla
PCo3
PCo1
B
log2(Fold change)
log2(Mean TPM)
C
Gene numbers
p.adjust
glucose metabolic process
gluconeogenesis
glutamine family amino acid biosynthetic process
L-glutamate import across plasma membrane
channel regulator activity
amino acid transport
social behavior
learning or memory
cognition
regulation of synapse organization
regulation of synapse structure or activity
regulation of synaptic transmission, glutamatergic
excitatory synapse
forebrain neuron differentiation
central nervous system neuron development
forebrain generation of neurons
GABAergic neuron differentiation
regulation of apoptotic signaling pathway
antigen processing and presentation via MHC class II
chemokine-mediated signaling pathway
regulation of interleukin-6 production
D
NSC-Vector
NSC-Rimkla
Slc1a2
Slc1a3
mGlur3
Gls
Gls2
Glud1
Ngfr
Syt4
Npas4
Kcnj3
Slc4a10
Nrp2

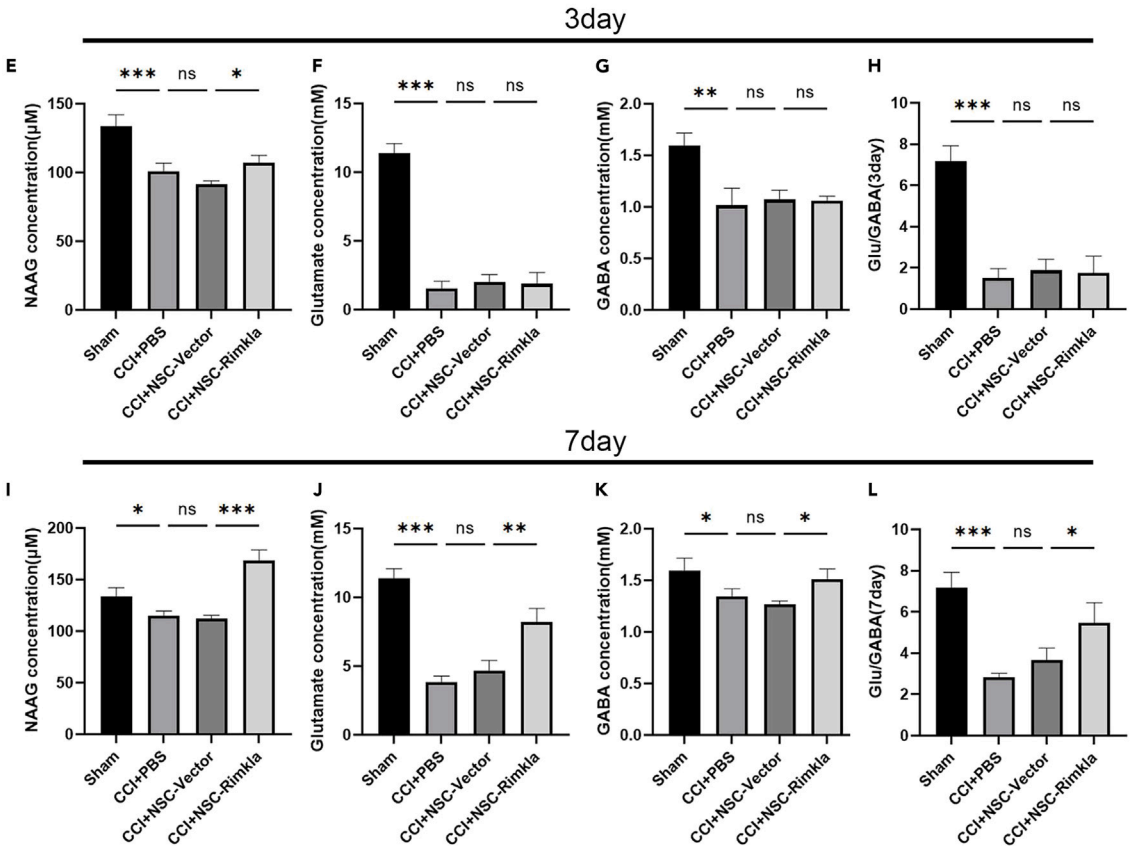
3day
E
NAAG concentration(μM)
F
Glutamate concentration(mM)
G
GABA concentration(mM)
H
Glu/GABA(3day)
7day
I
NAAG concentration(μM)
J
Glutamate concentration(mM)
K
GABA concentration(mM)
L
Glu/GABA(7day)
Sham
CCI+PBS
CCI+NSC-Vector
CCI+NSC-Rimkla

Figure 5. Grafted mNSCs overexpressing *Rimkla* activated glutamate metabolism related pathways

(A–D) Transcriptome sequencing results of hippocampal tissues on the injured side of NSC-Vector and NSC-*Rimkla* groups. (n = 3 per group) (A) PCoA analysis shows the distribution of dimensionality reduction in the two groups of samples.

(B) M-versus-A plot shows the differences in gene expression between the two groups of samples.

(C) KEGG enrichment analysis results of differential genes in the two groups.

(D) Heatmap of expression of genes related to glutamate metabolism and synaptic development in the two groups of samples.

(E–L) LC-MS/MS was used to measure the total contents of NAAG, glutamate, and GABA in the injured hippocampus of mice (n = 3 per group).

(E–G) contents of NAAG, glutamate and GABA in hippocampus at 3 days after transplantation.

(H) Glutamate/GABA ratio in hippocampus of mice on day 3 after transplantation.

(I–K) Contents of NAAG, glutamate, and GABA in hippocampus 7 days after transplantation.

(L) Glutamate/GABA ratio in hippocampus of mice on day 7 after transplantation. The error bars represent the S.E.M. *p < 0.05, **p < 0.01, ***p < 0.001.

activation of microglia and astrocytes produce a series of inflammatory responses.[20–22] Changes of these nerve cells in the hippocampus was examined on the 3rd and 7th day after transplantation. No significant difference was found in neurons, microglia, and astrocytes between the mNSCs group and the PBS group on the 3rd day. Compared with the Sham group, the expression of Tuj1 was decreased and the expressions of Gfap and Iba1 were increased in the injury group (Figure S2). However, some interesting changes occurred on the 7th day (Figure 3). The expression of Tuj1 in the NSC-Vector group and NSC-*Rimkla* group was significantly higher than the PBS group, which may be on account of the neuroprotective factors released by mNSCs[16,23] and the cell replacement effect of mNSCs.[24] In addition, the expression of Gfap in the mNSCs group was lower than the PBS group, which was consistent with previous researches that NSCs transplantation could regulate astrocytes after TBI.[25] Notably, due to the innate immune response caused by cell death after transplantation or exogenous transplantation,[26] grafted mNSCs led to microglia proliferation on the 7th day, but the overexpression of *Rimkla* can effectively alleviate this process, which may be related to enhanced transmitter communication, but further studies are needed to confirm and explain this phenomenon.

Although there was no significant difference in the number of neurons in the hippocampus between the NSC-Vector group and the NSC-*Rimkla* group on the 7th day, we unexpectedly found that the synapses in the hippocampal CA3 region of the NSC-*Rimkla* group were more intact and the density of dendritic spines was higher than the NSC-Vector group. The proportion of mushroom-shaped dendritic spines which represent mature dendritic spines was also higher in NSC-*Rimkla* group, suggesting that neuronal synaptic repair in CA3 region was promoted (Figure 4). Considering the important role of synapses and dendritic spines in learning and memory,[27,28] this finding also strongly explained why mice in NSC-*Rimkla*-OE group had better behavioral performance. However, it should be noted that there was no significant difference in the expression of synapse-associated proteins between NSC-Vector and NSC-*Rimkla* groups on the 3rd day (Figure S2). Considering the presynaptic release mechanism of NAAG[29–31] and the differentiation rule of NSCs,[10] we speculate that most neurons differentiated by mNSCs on the 3rd day after transplantation are not mature and their synapses were lack of normal function, resulting in the inability to release NAAG.

To confirm this hypothesis and reveal the mechanism by which NSC-*Rimkla*-OE transplantation promoted synaptic repair, total contents of NAAG, glutamate, GABA, and NAA in the hippocampus of lesion side in each group were measured on the 3rd and 7th day by LC-MS/MS. Whole transcriptome sequencing of hippocampus was also performed on the 7th day (Figure 5). The increase in NAAG in the NSC-*Rimkla*-OE group was more pronounced than other CCI groups. The enrichment analysis of differential genes involved in learning and memory, cognition, synaptic regulation, and neuronal differentiation, which was highly consistent with the results of previous studies. In particular, we also found significant alterations in the expression of genes involved in glutamate metabolism and transport. Many studies have confirmed that the concentration of glutamate in the synaptic cleft of neurons increases sharply within 24 h after TBI and maintains at a high level in the next few days,[32] which continues to mediate the excitotoxic injury of postsynaptic neurons.[33,34] However, the total glutamate concentration in the brain tissue around the injured area was lower than the Sham group on the 7th day after TBI,[35] which would lead to abnormal glutamate-glutamine cycle, affecting neuronal metabolism and development, and lead to synaptic dysfunction and neurodegeneration.[36] Therefore, we suggested that NAAG may play a neuroprotective role in the acute/subacute phase of TBI mainly by regulating glutamate transport to enhance support for neuronal metabolism and reduce postsynaptic excitotoxicity. This speculation was confirmed by our experiments. The total glutamate concentration in the hippocampus of the lesion side in all CCI groups was lower than the Sham group on the 3rd and 7th day post transplantation, while glutamate in NSC-*Rimkla*-OE group was significantly more than other CCI groups on the 7th day, and the glutamate/GABA ratio in NSC-*Rimkla*-OE group was closer to the Sham group. This confirmed the recovery of glutamate metabolism and circulation in the lesion side of hippocampus in NSC-*Rimkla*-OE group.

Further study on the expression of glutamate metabolism related genes showed that Slc1a2 had the most significant change. Slc1a2, also known as EAAT2/Glt-1, are sodium- and potassium-dependent members of the solute carrier family 6 (SLC1). In the nervous system, it is mainly expressed on the membrane surface of hippocampal astrocytes[37] and plays an important role in inhibiting excessive excitatory neurotransmission between synapses and providing glutamate to cells throughout the brain for metabolic purposes.[38] Many studies in animal TBI models have shown that Slc1a2 expression on the surface of astrocytes is down-regulated in the acute/subacute phase after TBI, resulting in increased intersynaptic glutamate levels and excitotoxicity.[39,40] Activation of mGlur3 can promote Slc1a2 activation on the surface of astrocytes.[41,42] The temporal and spatial relationship between mGluR3 and Slc1a2 in the hippocampus on the 3rd and 7th day post transplantation was further investigated. There was no significant difference in the protein expression of mGlur3 and Slc1a2 among all CCI groups on the 3rd day, however, the expression of these two proteins was significantly increased in the NSC-*Rimkla* group on the 7th day (Figures 6 and S3). It was suggested that the expression of these two proteins is closely related to the concentration of NAAG. We simultaneously labeled mGlur3

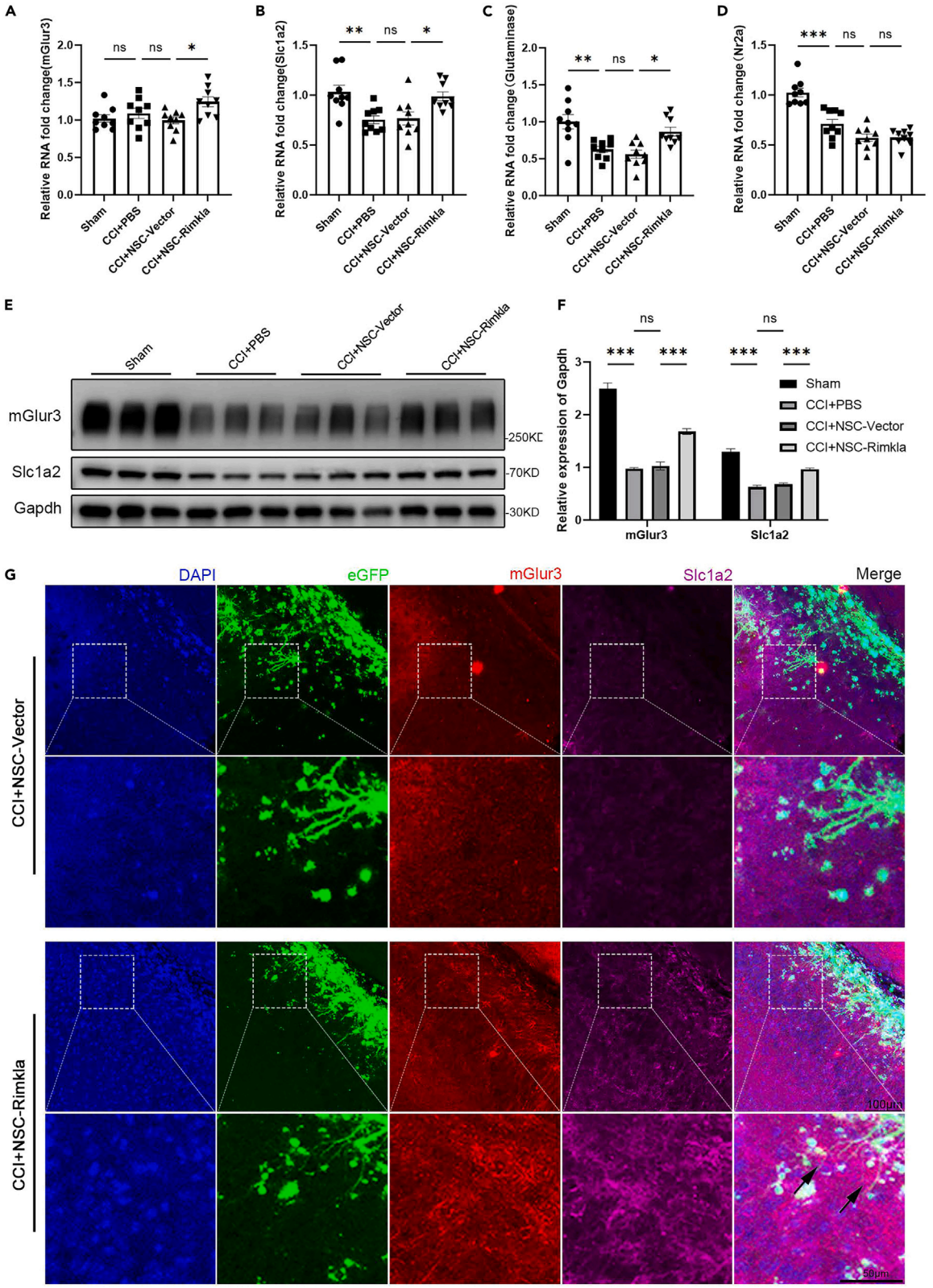
A
Relative RNA fold change(mGlur3)
ns
ns
*
Sham
CCI+PBS
CCI+NSC-Vector
CCI+NSC-Rimkla
B
Relative RNA fold change(Slc1a2)
**
ns
*
C
Relative RNA fold change (Glutaminase)
**
ns
*
D
Relative RNA fold change (Nr2a)
***
ns
ns
E
Sham
CCI+PBS
CCI+NSC-Vector
CCI+NSC-Rimkla
mGlur3
Slc1a2
Gapdh
250KD
70KD
30KD
F
Relative expression of Gapdh
ns
ns
***
***
***
***
Sham
CCI+PBS
CCI+NSC-Vector
CCI+NSC-Rimkla
mGlur3
Slc1a2
G
DAPI
eGFP
mGlur3
Slc1a2
Merge
CCI+NSC-Vector
CCI+NSC-Rimkla
100μm
50μm

Figure 6. mGlur3 and slc1a2 on the surface of astrocytes were activated near eGFP$^+$ synaptic terminals

(A–D) RT-qPCR was used to detect the mRNA expression of mGluR3, Slc1a2, Glutaminase and Nr2a in the injured hippocampus of the Sham, CCI+PBS, CCI+NSC-Vector, and CCI+NSC-*Rimkla* groups on day 7 after transplantation (n = 9 per group).

(E–G) The expression of mGluR3 and Slc1a2 protein in the injured hippocampus of mice in each group was detected by western blot on day 7 after transplantation. Right panel (F) quantizes and statistics band gray level and area. (n = 3 per group) (G) immunofluorescence and laser confocal scanning. DAPI (blue) marks nuclei, eGFP (green) marks transplanted cells, red marks anti-mglur3-positive protein, and purple marks anti-SLC1A2-positive protein. Black arrows mark mGlur3 and Slc1a2 co-expressing cells. Low power field Scale bar, 100μm. High power field Scale bar, 50μm. The error bars represent the S.E.M. *p < 0.05, **p < 0.01, ***p < 0.001.

and Slc1a2 in brain slices to observe the spatial relationship between them. A significant increase in mGlur3 and Slc1a2 expression in astrocytes near eGFP$^+$ synaptic terminals was observed in the NSC-*Rimkla*-OE group on the 7th day, whereas a similar phenomenon was not observed in the NSC-Vector group, confirming that NAAG activated mGlur3 and Slc1a2 on the surface of astrocytes. In addition, RT-qPCR demonstrated that the expression of glutaminase in NSC-*Rimkla*-OE group was also significantly increased. In summary, we suggested that NAAG released by mature neurons differentiated by grafted mNSCs promoted glutamate-glutamine transport between astrocytes and neurons in the hippocampus during the subacute phase of TBI. It is estimated that a single mouse cortical astrocyte can contact more than 100,000 synapses, while human astrocytes can contact as many as 2 million synapses.[43] We demonstrated that transplanted mNSCs could communicate with a large number of astrocytes, and then the neuroprotective effect of grafted *Rimkla*-overexpressing mNSCs tended to be considerable.

Interestingly, a significant enhancement of mGlur3 and Slc1a2 signaling in astrocytes was observed near eGFP$^+$ synaptic terminals, which supports the concept of a "tripartite synapse" from the side. The modern view is that the tripartite synapse mainly consists of slow and long-reaching modulation of neuronal activity, non-vesicular release of gliotransmitters, astrocyte driven regulation of synaptic homeostasis.[44] As shown in (Figure 7), the presynaptic membrane, postsynaptic membrane, and adjacent astrocytes form a "tripartite synapse" structure. Glutamate receptors and transporters on the surface of astrocytes respond to changes in intracellular ion concentration and dynamic changes in the balance of extracellular transmitters in real time, coordinating to maintain glutamate homeostasis between synapses. After TBI, the expression of glutamate transporters (Slc1a2, Slc1a3) on the surface of astrocytes is down-regulated, resulting in the accumulation and concentration of glutamate at synapses, resulting in excitotoxicity.[40] At the same time, it causes glutamate-glutamine cycling disorder between astrocytes and neurons, leading to neuronal deficits including altered neurotransmitter metabolism and synaptic function.[45,46] Besides, abnormalities in neuronal glutamate-glutamine metabolism also affect astrocyte glycolysis and neuronal lactate metabolism.[47,48]

In summary, the neuroprotective effects of grafted mNSCs overexpressing the NAAG synthetase II (*Rimkla*) were investigated. It was confirmed that NAAG released from the synaptic terminals of mature neurons differentiated from grafted *Rimkla*-overexpressing mNSCs activated mGlur3 on the surface of adjacent astrocytes, which in turn activated glutamate transporter Slc1a2, and enhanced glutamate transport from synaptic cleft to the astrocytes and glutamine synthesis. Therefore, it regulated glutamate-glutamine cycling between adjacent astrocytes and neurons in the subacute phase of CCI, thereby reducing excitotoxicity and enhancing support for neuronal metabolism and promoting neuronal synaptic repair in the hippocampal CA3 region, and ultimately facilitated cognitive recovery after TBI.

Limitations of the study

Notably, astrocytes play a positive role in the development and plasticity of neuronal synapses,[49] and mGluR3 activation can promote astrocyte survival and regulate astrocyte function.[42,50] Although we explored the effect of mGluR3 activation on Slc1a2 on the surface of astrocytes, the possibility that mGluR3 directly regulates the synaptic protective function of astrocytes was ignored, which pointed out a direction for subsequent research.

STAR★METHODS

Detailed methods are provided in the online version of this paper and include the following:

- KEY RESOURCES TABLE
- RESOURCE AVAILABILITY
  - Lead contact
  - Materials availability
  - Date and code availability
- EXPERIMENTAL MODEL AND STUDY PARTICIPANT DETAILS
- METHOD DETAILS
  - TBI procedure
  - Extraction and culture of mouse embryonic neural stem cells (mNSCs)
  - Differentiation of mNSCs *in vitro*
  - Lentivirus packaging and infection
  - Stereotaxic brain injection
  - Tissue section
  - Western blot

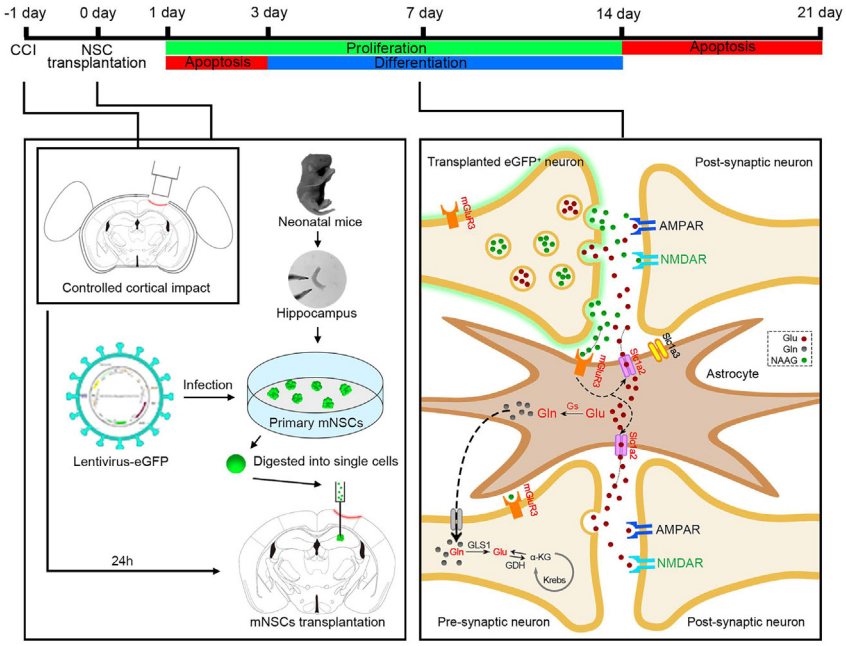

Figure 7. We transplanted *Rimkla* overexpression/knockdown mNSCs into mouse hippocampus 24 h after TBI induced by controlled cortical impact (CCI) and tracked the status of these grafted cells from day 1 to day 21 post transplantation

mNSCs proliferated actively from day 1 to day 14, differentiated gradually from day 3 to day 7, and gradually apoptotic from day 14 to day 21. mNSCs overexpressing *Rimkla* differentiated into eGFP^{+} neurons and participated in local neural circuits on the 7th day post transplantation. The release of NAAG in eGFP^{+} neurons activated mGlur3 on the surface of adjacent astrocytes and glutamate transporter Slc1a2 was then activated, which enhanced the glutamate transport from adjacent synapses to astrocytes and reduced the excitotoxicity of postsynaptic neurons caused by over-activation of NMDAR. Glutamate transported into astrocytes was converted to glutamine through the tricarboxylic acid cycle pathway and transported to neighboring neurons, which enhanced the nutritional metabolic support of neurons in the subacute phase after TBI.

- Real-Time qPCR
- Immunofluorescence
- Immunohistochemistry
- Morris water maze
- RNA isolation and sequencing
- Bioluminescence imaging
- Liquid chromatography and mass spectrometry (LC-MS/MS)
- Golgi staining

- QUANTIFICATION AND STATISTICAL ANALYSIS

SUPPLEMENTAL INFORMATION

Supplemental information can be found online at https://doi.org/10.1016/j.isci.2023.107913.

ACKNOWLEDGMENTS

This research was supported by grants from the National Natural Science Foundation of China (82271406, 82172820, 81771332 and 81571184), the Fundamental Research for the Central University, the Natural Science Foundation of Shanghai (22ZR1451200 and 22ZR1466200), the Key Disciplines Group Construction Project of Shanghai Pudong New Area Health Commission (PWZxq2022-10), the Medical Discipline Construction Project of Pudong Health Committee of Shanghai (PWYgy 2021-07) and the Outstanding Leaders Training Program of Pudong Health Bureau of Shanghai (PWR12018-07).

AUTHOR CONTRIBUTIONS

C.Z., J.Z., and M.L. designed experiments, interpreted results, and wrote the paper, T.J. conducted experiments and analyzed data. Y.P., M.C., and R.W. helped animal experiments. X.C. and C.Z. participated in cell and molecular studies. M.L. provided technical support for data analysis.

DECLARATION OF INTERESTS

The authors declare no competing interests.

Received: May 15, 2023
Revised: July 22, 2023
Accepted: September 12, 2023
Published: September 14, 2023

REFERENCES

1. Maas, A.I.R., Stocchetti, N., and Bullock, R. (2008). Moderate and severe traumatic brain injury in adults. Lancet Neurol. *7*, 728–741. https://doi.org/10.1016/S1474-4422(08)70164-9.
2. Akamatsu, Y., and Hanafy, K.A. (2020). Cell Death and Recovery in Traumatic Brain Injury. Neurotherapeutics *17*, 446–456. https://doi.org/10.1007/s13311-020-00840-7.
3. Meldrum, B.S. (2000). Glutamate as a neurotransmitter in the brain: review of physiology and pathology. J. Nutr. *130*, 1007S–1015S. https://doi.org/10.1093/jn/130.4.1007S.
4. Neale, J.H., Bzdega, T., and Wroblewska, B. (2000). N-Acetylaspartylglutamate: the most abundant peptide neurotransmitter in the mammalian central nervous system. J. Neurochem. *75*, 443–452. https://doi.org/10.1046/j.1471-4159.2000.0750443.x.
5. Morland, C., and Nordengen, K. (2022). N-Acetyl-Aspartyl-Glutamate in Brain Health and Disease. Int. J. Mol. Sci. *23*, 1268. https://doi.org/10.3390/ijms23031268.
6. Neale, J.H., Olszewski, R.T., Zuo, D., Janczura, K.J., Profaci, C.P., Lavin, K.M., Madore, J.C., and Bzdega, T. (2011). Advances in understanding the peptide neurotransmitter NAAG and appearance of a new member of the NAAG neuropeptide family. J. Neurochem. *118*, 490–498. https://doi.org/10.1111/j.1471-4159.2011.07338.x.
7. Zhong, C., Zhao, X., Sarva, J., Kozikowski, A., Neale, J.H., and Lyeth, B.G. (2005). NAAG peptidase inhibitor reduces acute neuronal degeneration and astrocyte damage following lateral fluid percussion TBI in rats. J. Neurotrauma *22*, 266–276. https://doi.org/10.1089/neu.2005.22.266.
8. Zhong, C., Zhao, X., Van, K.C., Bzdega, T., Smyth, A., Zhou, J., Kozikowski, A.P., Jiang, J., O'Connor, W.T., Berman, R.F., et al. (2006). NAAG peptidase inhibitor increases dialysate NAAG and reduces glutamate, aspartate and GABA levels in the dorsal hippocampus following fluid percussion injury in the rat. J. Neurochem. *97*, 1015–1025. https://doi.org/10.1111/j.1471-4159.2006.03786.x.
9. Gao, Y., Xu, S., Cui, Z., Zhang, M., Lin, Y., Cai, L., Wang, Z., Luo, X., Zheng, Y., Wang, Y., et al. (2015). Mice lacking glutamate carboxypeptidase II develop normally, but are less susceptible to traumatic brain injury. J. Neurochem. *134*, 340–353. https://doi.org/10.1111/jnc.13123.
10. Wang, Z., Wang, Y., Wang, Z., Zhao, J., Gutkind, J.S., Srivatsan, A., Zhang, G., Liao, H.S., Fu, X., Jin, A., et al. (2015). Polymeric Nanovehicle Regulated Spatiotemporal Real-Time Imaging of the Differentiation Dynamics of Transplanted Neural Stem Cells after Traumatic Brain Injury. ACS Nano *9*, 6683–6695. https://doi.org/10.1021/acsnano.5b00690.
11. Hayashi, Y., Lin, H.T., Lee, C.C., and Tsai, K.J. (2020). Effects of neural stem cell transplantation in Alzheimer's disease models. J. Biomed. Sci. *27*, 29. https://doi.org/10.1186/s12929-020-0622-x.
12. Smith, D.H., Soares, H.D., Pierce, J.S., Perlman, K.G., Saatman, K.E., Meaney, D.F., Dixon, C.E., and McIntosh, T.K. (1995). A model of parasagittal controlled cortical impact in the mouse: cognitive and histopathologic effects. J. Neurotrauma *12*, 169–178. https://doi.org/10.1089/neu.1995.12.169.
13. Tucker, L.B., Velosky, A.G., and McCabe, J.T. (2018). Applications of the Morris water maze in translational traumatic brain injury research. Neurosci. Biobehav. Rev. *88*, 187–200. https://doi.org/10.1016/j.neubiorev.2018.03.010.
14. Blurton-Jones, M., Kitazawa, M., Martinez-Coria, H., Castello, N.A., Müller, F.J., Loring, J.F., Yamasaki, T.R., Poon, W.W., Green, K.N., and LaFerla, F.M. (2009). Neural stem cells improve cognition via BDNF in a transgenic model of Alzheimer disease. Proc. Natl. Acad. Sci. USA *106*, 13594–13599. https://doi.org/10.1073/pnas.0901402106.
15. Lee, I.S., Jung, K., Kim, I.S., Lee, H., Kim, M., Yun, S., Hwang, K., Shin, J.E., and Park, K.I. (2015). Human neural stem cells alleviate Alzheimer-like pathology in a mouse model. Mol. Neurodegener. *10*, 38. https://doi.org/10.1186/s13024-015-0035-6.
16. Xiong, L.L., Hu, Y., Zhang, P., Zhang, Z., Li, L.H., Gao, G.D., Zhou, X.F., and Wang, T.H. (2018). Neural Stem Cell Transplantation Promotes Functional Recovery from Traumatic Brain Injury via Brain Derived Neurotrophic Factor-Mediated Neuroplasticity. Mol. Neurobiol. *55*, 2696–2711. https://doi.org/10.1007/s12035-017-0551-1.
17. Zibara, K., Ballout, N., Mondello, S., Karnib, N., Ramadan, N., Omais, S., Nabbouh, A., Caliz, D., Clavijo, A., Hu, Z., et al. (2019). Combination of drug and stem cells neurotherapy: Potential interventions in neurotrauma and traumatic brain injury. Neuropharmacology *145*, 177–198. https://doi.org/10.1016/j.neuropharm.2018.09.032.
18. Pang, A.L., Xiong, L.L., Xia, Q.J., Liu, F., Wang, Y.C., Liu, F., Zhang, P., Meng, B.L., Tan, S., and Wang, T.H. (2017). Neural Stem Cell Transplantation Is Associated with Inhibition of Apoptosis, Bcl-xL Upregulation, and Recovery of Neurological Function in a Rat Model of Traumatic Brain Injury. Cell Transplant. *26*, 1262–1275. https://doi.org/10.1177/0963689717715168.
19. Forbes, M.L., Clark, R.S., Dixon, C.E., Graham, S.H., Marion, D.W., DeKosky, S.T., Schiding, J.K., and Kochanek, P.M. (1998). Augmented neuronal death in CA3 hippocampus following hyperventilation early after controlled cortical impact. J. Neurosurg. *88*, 549–556. https://doi.org/10.3171/jns.1998.88.3.0549.
20. Jassam, Y.N., Izzy, S., Whalen, M., McGavern, D.B., and El Khoury, J. (2017). Neuroimmunology of Traumatic Brain Injury: Time for a Paradigm Shift. Neuron *95*, 1246–1265. https://doi.org/10.1016/j.neuron.2017.07.010.
21. Corps, K.N., Roth, T.L., and McGavern, D.B. (2015). Inflammation and neuroprotection in traumatic brain injury. JAMA Neurol. *72*, 355–362. https://doi.org/10.1001/jamaneurol.2014.3558.
22. Burda, J.E., and Sofroniew, M.V. (2014). Reactive gliosis and the multicellular response to CNS damage and disease. Neuron *81*, 229–248. https://doi.org/10.1016/j.neuron.2013.12.034.
23. Sun, M.K., Passaro, A.P., Latchoumane, C.F., Spellicy, S.E., Bowler, M., Goeden, M., Martin, W.J., Holmes, P.V., Stice, S.L., and Karumbaiah, L. (2020). Extracellular Vesicles Mediate Neuroprotection and Functional Recovery after Traumatic Brain Injury. J. Neurotrauma *37*, 1358–1369. https://doi.org/10.1089/neu.2019.6443.
24. Kopach, O., Rybachuk, O., Krotov, V., Kyryk, V., Voitenko, N., and Pivneva, T. (2018). Maturation of neural stem cells and integration into hippocampal circuits - a functional study in an *in situ* model of cerebral ischemia. J. Cell Sci. *131*, jcs210989. https://doi.org/10.1242/jcs.210989.
25. Nasser, M., Ballout, N., Mantash, S., Bejjani, F., Najdi, F., Ramadan, N., Soueid, J., Zibara, K., and Kobeissy, F. (2018). Transplantation of Embryonic Neural Stem Cells and Differentiated Cells in a Controlled Cortical Impact (CCI) Model of Adult Mouse Somatosensory Cortex. Front. Neurol. *9*, 895. https://doi.org/10.3389/fneur.2018.00895.
26. Reekmans, K., De Vocht, N., Praet, J., Fransen, E., Le Blon, D., Hoornaert, C., Daans, J., Goossens, H., Van der Linden, A., Berneman, Z., and Ponsaerts, P. (2012). Spatiotemporal evolution of early innate immune responses triggered by neural stem cell grafting. Stem Cell Res. Ther. *3*, 56. https://doi.org/10.1186/scrt147.
27. Lichtman, J.W., and Colman, H. (2000). Synapse elimination and indelible memory. Neuron *25*, 269–278. https://doi.org/10.1016/s0896-6273(00)80893-4.
28. Yang, G., Pan, F., and Gan, W.B. (2009). Stably maintained dendritic spines are associated with lifelong memories. Nature *462*, 920–924. https://doi.org/10.1038/nature08577.
29. Williamson, L.C., and Neale, J.H. (1988). Ultrastructural localization of N-acetylaspartylglutamate in synaptic vesicles of retinal neurons. Brain Res. *456*, 375–381. https://doi.org/10.1016/0006-8993(88)90243-0.
30. Zollinger, M., Amsler, U., Do, K.Q., Streit, P., and Cuénod, M. (1988). Release of

N-acetylaspartylglutamate on depolarization of rat brain slices. J. Neurochem. *51*, 1919–1923. https://doi.org/10.1111/j.1471-4159.1988.tb01178.x.

31. Pittaluga, A., Barbeito, L., Serval, V., Godeheu, G., Artaud, F., Glowinski, J., and Chéramy, A. (1988). Depolarization-evoked release of N-acetyl-L-aspartyl-L-glutamate from rat brain synaptosomes. Eur. J. Pharmacol. *158*, 263–266. https://doi.org/10.1016/0014-2999(88)90076-3.
32. Dorsett, C.R., McGuire, J.L., DePasquale, E.A.K., Gardner, A.E., Floyd, C.L., and McCullumsmith, R.E. (2017). Glutamate Neurotransmission in Rodent Models of Traumatic Brain Injury. J. Neurotrauma *34*, 263–272. https://doi.org/10.1089/neu.2015.4373.
33. Carbonell, W.S., and Grady, M.S. (1999). Evidence disputing the importance of excitotoxicity in hippocampal neuron death after experimental traumatic brain injury. Ann. N. Y. Acad. Sci. *890*, 287–298. https://doi.org/10.1111/j.1749-6632.1999.tb08005.x.
34. Faden, A.I., Demediuk, P., Panter, S.S., and Vink, R. (1989). The role of excitatory amino acids and NMDA receptors in traumatic brain injury. Science *244*, 798–800. https://doi.org/10.1126/science.2567056.
35. Harris, J.L., Yeh, H.W., Choi, I.Y., Lee, P., Berman, N.E., Swerdlow, R.H., Craciunas, S.C., and Brooks, W.M. (2012). Altered neurochemical profile after traumatic brain injury: (1)H-MRS biomarkers of pathological mechanisms. J. Cerebr. Blood Flow Metabol. *32*, 2122–2134. https://doi.org/10.1038/jcbfm.2012.114.
36. Andersen, J.V., Schousboe, A., and Verkhratsky, A. (2022). Astrocyte energy and neurotransmitter metabolism in Alzheimer's disease: Integration of the glutamate/GABA-glutamine cycle. Prog. Neurobiol. *217*, 102331. https://doi.org/10.1016/j.pneurobio.2022.102331.
37. Palacín, M., Estévez, R., Bertran, J., and Zorzano, A. (1998). Molecular biology of mammalian plasma membrane amino acid transporters. Physiol. Rev. *78*, 969–1054. https://doi.org/10.1152/physrev.1998.78.4.969.
38. Kanai, Y., Clémençon, B., Simonin, A., Leuenberger, M., Lochner, M., Weisstanner, M., and Hediger, M.A. (2013). The SLC1 high-affinity glutamate and neutral amino acid transporter family. Mol. Aspect. Med. *34*, 108–120. https://doi.org/10.1016/j.mam.2013.01.001.
39. van Landeghem, F.K.H., Weiss, T., Oehmichen, M., and von Deimling, A. (2006). Decreased expression of glutamate transporters in astrocytes after human traumatic brain injury. J. Neurotrauma *23*, 1518–1528. https://doi.org/10.1089/neu.2006.23.1518.
40. Pajarillo, E., Rizor, A., Lee, J., Aschner, M., and Lee, E. (2019). The role of astrocytic glutamate transporters GLT-1 and GLAST in neurological disorders: Potential targets for neurotherapeutics. Neuropharmacology *161*, 107559. https://doi.org/10.1016/j.neuropharm.2019.03.002.
41. Yao, H.H., Ding, J.H., Zhou, F., Wang, F., Hu, L.F., Sun, T., and Hu, G. (2005). Enhancement of glutamate uptake mediates the neuroprotection exerted by activating group II or III metabotropic glutamate receptors on astrocytes. J. Neurochem. *92*, 948–961. https://doi.org/10.1111/j.1471-4159.2004.02937.x.
42. Battaglia, G., Riozzi, B., Bucci, D., Di Menna, L., Molinaro, G., Pallottino, S., Nicoletti, F., and Bruno, V. (2015). Activation of mGlu3 metabotropic glutamate receptors enhances GDNF and GLT-1 formation in the spinal cord and rescues motor neurons in the SOD-1 mouse model of amyotrophic lateral sclerosis. Neurobiol. Dis. *74*, 126–136. https://doi.org/10.1016/j.nbd.2014.11.012.
43. Allen, N.J., and Eroglu, C. (2017). Cell Biology of Astrocyte-Synapse Interactions. Neuron *96*, 697–708. https://doi.org/10.1016/j.neuron.2017.09.056.
44. Lalo, U., Koh, W., Lee, C.J., and Pankratov, Y. (2021). The tripartite glutamatergic synapse. Neuropharmacology *199*, 108758. https://doi.org/10.1016/j.neuropharm.2021.108758.
45. Andersen, J.V., Markussen, K.H., Jakobsen, E., Schousboe, A., Waagepetersen, H.S., Rosenberg, P.A., and Aldana, B.I. (2021). Glutamate metabolism and recycling at the excitatory synapse in health and neurodegeneration. Neuropharmacology *196*, 108719. https://doi.org/10.1016/j.neuropharm.2021.108719.
46. Cheung, G., Bataveljic, D., Visser, J., Kumar, N., Moulard, J., Dallérac, G., Mozheiko, D., Rollenhagen, A., Ezan, P., Mongin, C., et al. (2022). Physiological synaptic activity and recognition memory require astroglial glutamine. Nat. Commun. *13*, 753. https://doi.org/10.1038/s41467-022-28331-7.
47. Magistretti, P.J., and Pellerin, L. (1999). Cellular mechanisms of brain energy metabolism and their relevance to functional brain imaging. Philos. Trans. R. Soc. Lond. B Biol. Sci. *354*, 1155–1163. https://doi.org/10.1098/rstb.1999.0471.
48. Dienel, G.A. (2019). Brain Glucose Metabolism: Integration of Energetics with Function. Physiol. Rev. *99*, 949–1045. https://doi.org/10.1152/physrev.00062.2017.
49. Blanco-Suárez, E., Caldwell, A.L.M., and Allen, N.J. (2017). Role of astrocyte-synapse interactions in CNS disorders. J. Physiol. *595*, 1903–1916. https://doi.org/10.1113/JP270988.
50. Durand, D., Carniglia, L., Caruso, C., and Lasaga, M. (2013). mGlu3 receptor and astrocytes: partners in neuroprotection. Neuropharmacology *66*, 1–11. https://doi.org/10.1016/j.neuropharm.2012.04.009.

STAR★METHODS

KEY RESOURCES TABLE

REAGENT or RESOURCE	SOURCE	IDENTIFIER
Antibodies		
Rabbit anti-GFAP	CellSignalingTechnology	Cat#80788S; RRID:AB_2799963
Chicken anti-GFAP	Abcam	Cat#ab4674; RRID:AB_304558
Mouse anti-EAAT2	SANTA CRUZ	Cat#sc-365634; RRID:AB_10844832
Rabbit anti-mGLUR3	Abcam	Cat#ab281922; RRID:AB_2943412
Chicken anti-Nestin	Abcam	Cat#ab134017; RRID:AB_2753197
Rabbit anti-β3-Tubulin	Affinity	Cat#AF7000; RRID:AB_2846220
Rabbit anti-Map2	Proteintech	Cat#17490-1-AP; RRID:AB_2137880
Rabbit anti-*Rimkla*	GeneTex	Cat#GTX87628; RRID:AB_10723973
Rabbit anti-Iba1	CellSignalingTechnology	Cat#17198; RRID:AB_2820254
Rabbit anti-PSD95	CellSignalingTechnology	Cat#37657; RRID:AB_2943447
Rabbit anti-GAPDH	Affinity	Cat#AF7021; RRID:AB_2839421
Rabbit anti-beta Actin	Affinity	Cat#AF7018; RRID:AB_2839420
Rabbit anti-Olig2	Abcam	Cat#ab136253; RRID:AB_2810961
Goat Anti-Rabbit IgG HRP	Affinity	Cat#S0001; RRID:AB_2839429
Goat Anti-Mouse IgG HRP	Affinity	Cat#S0002; RRID:AB_2839430
Rabbit Anti-Chicken IgG HRP	Proteintech	Cat#SA00001-6; RRID:AB_2890885
Goat Anti-Mouse AlexaFluor 488	Jackson	Cat#115-545-003; RRID:AB_2338840
Goat Anti-Mouse AlexaFluor 647	Jackson	Cat#115-605-003; RRID:AB_2338902
Goat Anti-Rabbit AlexaFluor 594	Jackson	Cat#111-585-003; RRID:AB_2338059
Rabbit Anti-Chicken AlexaFluor 647	Jackson	Cat#303-605-003; RRID:AB_2339335
Bacterial and virus strains		
PGMLV-6751	Genomeditech Co.	
pGMLV-SC5	Genomeditech Co.	
Chemicals, peptides, and recombinant proteins		
EGF	Sigma	Cat#62253-63-8
bFGF	Sigma	Cat#GF003AF
Poly-L-Ornitihine	Sigma	Cat#27378-49-0
Laminin	Sigma	Cat#114956-81-9
GlutaMAX-I	Gibco	Cat#A1286001
dibutyryl cAMP	Sigma	Cat#16980-89-5
3,3 ', 5-Triiodo-L-thyronine sodium	Sigma	Cat#55-06-1
N-acetyl aspartyl-glutamate	Sigma	Cat#A5930
N-acetyl-aspartate	Sigma	Cat#00920
L-Glutamate	Sigma	Cat#G1251
γ-Aminobutyric acid	Sigma	Cat#A2129

(*Continued on next page*)

Continued

REAGENT or RESOURCE	SOURCE	IDENTIFIER
Critical commercial assays		
Immobilon Western	Millipore	Cat#WBKLS0500
PrimeScript™ RT reagent Kit	Takara	Cat#RR037A
TB Green® Premix Ex Taq™ II	Takara	Cat#RR820A
Deposited data		
Original, unprocessed data	This paper	https://doi.org/10.17632/5pd72p7n4m.1
Experimental models: Cell lines		
Mouse embryonic neural stem cells	This paper	
HEK 293T	ATCC	
Experimental models: Organisms/strains		
C57BL/6J	Beijing Vital River Laboratory Animal Technology Co.	
Oligonucleotides		
shRNA oligo sequence	This study, see Table S1	
Primers for qPCR	This study, see Table S2	
Software and algorithms		
Prism 9	Graphpad	http://www.graphpad.com
Tracking Master	VanBi	
ImageJ/Fiji		https://imagej.nih.gov/ij/
R Project		https://www.r-project.org/
Other		
Mouse intracranial injection micropump system	MINICELL	
Pin-Point™ CCI device	Hatteras Instruments Inc.	Model PCI3000
Vibrating microtome	Leica	VT1200S
IVIS Spectrum imaging system	PerkinElmer Inc.	

RESOURCE AVAILABILITY

Lead contact

Further information and requests for resources and reagents should be directed to and will be fulfilled by the lead contact, Chunlong Zhong (drchunlongzhong@tongji.edu.cn).

Materials availability

Plasmids generated in this study are available from the lead contact upon request.

This study did not generate new unique reagents.

Date and code availability

- All data reported in this paper will be shared by the lead contact upon request.
- This paper does not report original code.
- Any additional information required to reanalyze the data reported in this paper is available from the lead contact upon request.

EXPERIMENTAL MODEL AND STUDY PARTICIPANT DETAILS

Healthy 7 weeks old male C57BL/6J mice (from Beijing Vital River Laboratory Animal Technology Co.) weighing between 18g-26g were selected in this experiment. All mice had been kept in a suitable environment with free access to food and water. Light/dark altered every 12 hours. All animal experiments were approved by the Animal Care and Use Committee of Tongji University School of Medicine.

METHOD DETAILS

TBI procedure

In this experiment, moderate controlled cortical impact (CCI) was performed using Pin-Point™ CCI device (Model PCI3000, Hatteras Instruments Inc., USA), and mice were divided into Sham and CCI groups. Sodium pentobarbital (50mg/kg) was injected intraperitoneally for anesthesia, and the head of the mouse was fixed in a stereotaxic frame after the foot reflex had disappeared. Iodophor was used to disinfect the skin, the scalp was cut open to expose the skull, a 3.5-mm diameter window was then opened using a skull drill at 2.0 mm lateral to the midline over the right hemisphere and 2.0 mm posterior to bregma. Impact tip diameter was 3mm, tilt angle was 15 degrees, impact velocity was 3m/s, depth was 1mm, and impact duration was 180ms. After the operation, the scalp was sutured and the mice were placed on a heating blanket to await resuscitation while the temperature was monitored with a rectal thermometer and body temperature was maintained at 37 degrees. The Sham group underwent the same surgical and anesthetic procedures except that CCI injury was not performed.

Extraction and culture of mouse embryonic neural stem cells (mNSCs)

mNSCs were isolated from the brain of C57BL/6 mice within 3 days post birth. Specific methods are briefly described as follows: neonatal mice were decapitated directly with scissors after induction of anesthesia with isoflurane. The heads were immersed in dissection buffer, and the bilateral hippocampal tissues were dissected out. The hippocampal tissues were crushed with ophthalmic scissors and then transferred to 1ml TrypLE (Gibco, USA) digestion solution. 3ml neural stem cell medium (DMEM/F12, B27 (Thermo, USA), EGF,bFGF, heparin, P/S, progesterone, putrescine, Hepes Buffer, 30% glucose (Sigma,USA)) were added. After centrifugation (1000r,5min), DNase was added, the supernatant was removed to a new EP tube after standing for 5min, and was resuspended in neural stem cell medium after centrifuging. Fluid was semi-quantitatively changed every other day, and mNSCs were subcultured after 7 days. After centrifugation, the supernatant was removed. The cells were resuspended in 1ml TrypLE and incubated at 37°C for 45min. NSCs medium and DNase were added. After centrifugation, the cells were resuspended in medium containing DNase and gently blown 3 times by a 1ml syringe. After centrifugation, mNSCs were resuspended and seeded into dishes.

Differentiation of mNSCs *in vitro*

Plates were coated with Poly-L-Ornitihine and Laminin. After the cells were digested, they were cultured in neural stem cell medium for 24 hours and then replaced with neuron-inducing(Neurobasal Media, 2mM GlutaMAX-I, 2% B-27 (Thermo), Four days later, dibutyryl cAMP (Sigma, USA) was added daily in the plate to a final concentration of 0.5 mM), astrocyte-inducing(Neurobasal media, GlutaMAX-I, 2% B-27, 3,3 ', 5-Triiodo-L-thyronine sodium, 30 ng/mL, (Sigma)), oligodendrocyte-inducing(DMEM, 2mM GlutaMAX-I, 1% N2-Supplement, 1% FBS)medium, respectively. Neural stem cells were cultured in specific media for 10 days before the next experiments.

Lentivirus packaging and infection

PGMLV-6751 overexpression vector and pGMLV-SC5 RNAi interference vector (Genomeditech Co., shanghai) were used as follows. Firstly, the target fragment was cut out through the restriction sites at both ends of the target fragment (shRNA oligo sequence is shown in Table S1), and the target fragment was connected into the overexpression or interference vector after the same digestion. The ligation product was transferred into the prepared competent bacterial cells, and the resulting monoclonal colonies were sequenced. The correct clone was defined as the successful construction of the overexpression or interference vector of the target gene. The constructed lentiviral vector and its auxiliary packaging original vector plasmid were co-transfected into HEK293T cells using HG transgene reagent. After 10-12 hours of transfection, enhancing buffer was added, followed by 8 hours of fresh medium, and the cell supernatant rich in lentiviral particles was collected after 48 hours of culture. The lentivirus was concentrated to obtain a high titer, and the virus titer was measured and calibrated in HEK293T cells. After mNSCs were cultured to the third day of the second generation, 10μL of lentivirus solution was added to the medium. After mNSCs were cultured to the third generation, 10 μl of lentivirus solution was added to the medium again. The medium was changed 48h after each addition of lentivirus. The efficiency of infection was determined by eGFP fluorescence under a fluorescence microscope.

Stereotaxic brain injection

24 hours after CCI, except for the sham group (n=25), other mice were randomly divided into CCI+PBS (n=35), CCI+NSC-Vector(n=35), CCI+NSC-*Rimkla*-OE(n=35) and CCI+NSC-*Rimkla*-shRNA (n=6) groups. PBS and corresponding gene-modified mNSCs were injected. The mice were anesthetized and immobilized using the same method as CCI. The mouse intracranial injection micropump system (MINICELL, Shanghai) and 10μL Hamilton microinjection needle was used. mNSC was digested into a single cell suspension, and 500 000 mNSC were resuspended in 5μL PBS and inhaled inside a microsyringe. After re-exposure of the exposed bone, the needles were inserted in the following positions: ML:1.75mm, AP: -2mm, DV: -1.75mm. The speed of injection was 0.25 μL /min. After the injection, the needle was retained for 5 minutes, and then again for 3 minutes after withdrawing 0.75mm of the needle. The scalp was sutured after the injection was completed. The injection was performed on a heating blanket at 36°C throughout.

Tissue section

Brain tissues were removed from mice after heart perfusion using 4% paraformaldehyde and immersed in 4% paraformaldehyde for 24 hours at 4°C. Brain tissue was subsequently embedded using 2% Agarose (Invitrogen, USA) and removed before sectioning. Sections were made

using a vibrating microtome (Leica VT1200S, German). The slice thickness was set to 30μm. After cutting into the appropriate position, the brain slices were removed and immersed in PBS for the next step.

Western blot

Mice were sacrificed by neck removal and hippocampal tissues were dissected. All tissue was added with 500 μL of pre-chilled RIPA lysate. After sonication, SDS-PAGE buffer(Beyotime, China) was added to the supernatant and the mixture was heated to 98°C for complete denaturation. The prepared sample was added 5μL to 10% precast glue and subsequently transferred to PVDF membrane after electrophoresis. The membrane was blocked with 5% BSA (Beyotime, China) for 2 hours, then was incubated with primary antibodies for 12 hours at 4°C on a shaker. The primary and secondary antibodies used in this experiment are listed in Table S3. After being washed three times with TBST, the membrane was incubated with the corresponding secondary antibody for 2 hours at room temperature on a shaker. Protein bands were then detected by western blot detection reagents (Millipore, Billerica, MA) and all images were acquired using the ChemiDoc Touch System. Images were quantified using ImageJ.

Real-Time qPCR

According to the manufacturer's protocol, total RNA was extracted using Trizol (Trizol™ Reagent, Invitrogen) and then was reverse transcribed into cDNA using PrimeScript™ RT reagent Kit (Takara, RR037A). Real-time qPCR(RT-qPCR) detection was performed with TB Green® Premix Ex Taq™ II (Takara, RR820A) using the QuantStudio 7 Flex Real-Time PCR System (Thermo, USA). The ΔΔCT method was used to calculate the relative gene expression levels. Primer sequences used in the experiment are listed in Table S2.

Immunofluorescence

Brain tissue sections were immersed in rupture solution containing 0.3%Triton-100 and 10% donkey serum for 1 h, followed by incubation with the corresponding primary antibody for 12 h at 4°C. Primary antibodies were eluted with PBST and incubated with the corresponding secondary antibodies for 2 hours at room temperature in the dark. See Table S3 for specific primary and secondary antibodies. After elution of secondary antibodies with PBST, brain slices were evenly spread on glass slides and sealed with an anti-fluorescence quencher containing DAPI.

Immunohistochemistry

Brain tissues were removed and embedded in paraffin before sectioning. Sections were deparaffinized in an oven and sequentially immersed in xylene and gradient concentrations of alcohol, followed by immersion in purified water for 10 min. This was followed by heating for 10 min in the environment of antigen repair solution. After three washes of PBST, 3% hydrogen peroxide was dropwise added to the tissue and incubated at room temperature in the dark for 20 minutes. 3% BSA was added and incubated for 1 hour. Primary antibodies (See Table S3) were added and sections were placed in a wet box for overnight incubation at 4°C. The next day, the sections were incubated with the corresponding secondary antibody for 1 hour at room temperature and eluted with PBST. DAB solution was used for staining.

Morris water maze

Morris water maze was used to evaluate learning and memory of mice 14 days after mNSCs transplantation. The water maze device is a circular pool with a diameter of 180 cm and a depth of 50cm, which is divided into four quadrants, NW, NE, SE and SW. The water temperature in the pool was maintained at 21 ± 1° C, and an escape platform with a diameter of 8cm was placed 1cm below the water surface and at an appropriate distance from the pool wall. There were fixed black visual cues above and around the pool. The pool is insulated from the outside world by a curtain that does not radiate light. In the place navigation test phase, the mouse was slowly placed into the water with its head facing the pool wall and allowed to explore the position of the platform. After finding the platform, the mouse was allowed to stay for 10 seconds, and if the platform was still not found after 90 seconds, the mouse was guided to the platform and stayed for 10 seconds. The time for each mouse to find the platform was recorded. After swimming, the mice were placed under an incandescent lamp to dry. Each mouse was trained four times a day with a different quadrant for each water entry and at least 30 min between sessions. The training lasted for 5 days. On day 6, the platform was removed for spatial probe test. Mice were placed in the quadrant opposite to the quadrant where the platform was located, and the performance of mice when looking for the platform was recorded for 60 seconds. The swimming process of mice was analyzed using Tracking Master (VanBi, Shanghai).

RNA isolation and sequencing

The hippocampus was dissected immediately after the mice were sacrificed by neck removal and snap-frozen in liquid nitrogen. Total RNA was extracted using Trizol (Sangon, Shanghai), and the quality of RNA samples was checked using a SMA4000 microspectrophotometer (Merinton, Beijing). The samples were then sent to Shanghai Sangon for sequencing on a NovaSeq6000 (Illumina San Diego CA, USA) platform. The results were analyzed using R software, mainly using "DESeq2", "enrichplot" and "clusterProfiler" packages for gene difference analysis and GO analysis. All p-values and q-values were set at 0.05.

Bioluminescence imaging

Bioluminescence imaging was performed using an IVIS Spectrum imaging system (PerkinElmer Inc., USA). The head hair of the mice was removed after anesthesia induced by isoflurane. The control group (injected with PBS) and the experimental group (injected with mNSCs) were placed in the imaging instrument in parallel for eGFP luminescence imaging. The signal intensity of the injection area was quantified.

Liquid chromatography and mass spectrometry (LC-MS/MS)

Tissue Preparation. A proper amount of mouse hippocampal Tissue was precisely weighed and mechanically homogenized with precooled normal saline, then 0.5ml was transferred to a new centrifuge tube, then mass spectrometric methanol was added and shaken for 1min. After 30min of low temperature sonication, the supernatant was taken and dried with nitrogen gas. After volume determination with 0.2ml ultrapure water, the mixture was centrifuged at 13000r/min for 15min. Supernatant was filtered with a 0.22 μm filter (Millipore Sigma, SLGP033R).

Reagents and chemicals. N-acetyl aspartyl-glutamate (NAAG, Sigma, A5930), N-acetyl-aspartate (NAA, Sigma, 00920), L-Glutamate (Glu, Sigma, G1251), γ-Aminobutyric acid (GABA, Sigma, A2129), Methanol (Macklin, M813904), Formic acid (Macklin, F875284), Acetonitrile (Macklin, A800366).

Standard sample preparation. The standard sample was precisely weighed to prepare a mixed standard linear mother solution with a concentration of 1μg/mL and then the solution was diluted with methanol to obtain a series of working solutions with concentrations of 100, 50, 25, 15, 5, 2.5, and 1.5ng/mL. The mother and working solutions for linear and quality control were stored at -20°C.

Liquid chromatography was performed on an ACQUITY UPLC HSS T3 column (1.8 × 100 mm, 2.1 μm particle size) at 30°C column temperature. Mobile phase consisted of (A) 0.1% formic acid and (B) ACN. Injection volume was 10 μL. The flow rate was set at 300 μL/min with 2 minutes in 99% solvent A and 1% solvent B followed by a gradient from 99% solvent A and 1% solvent B to 40% solvent A and 60% solvent B. LC-MS/MS analysis was performed on an AB Sciex API 4000 ™ LC/MS/MS triple quadrupole tandem mass spectrometer. MS parameters: The electrospray ionization source (ESI) was used in the negative ion ionization mode. The ion source temperature was set at 450°C, while the ion source voltage was -4500V. The curtain gas was maintained at 35 psi, and both the atomization gas and auxiliary gas were set at 60 psi. Multiple response monitoring (MRM) was used for scanning. Relative quantification of metabolites was performed based on peak areas.

Golgi staining

The mice were sacrificed on the 7th day after mNSCs transplantation, and their brains were removed and immersed in 4%PFA for 24 hours. The brains were cut into 3mm thick tissue blocks near the hippocampal plane and completely immersed in Golgi staining solution (haokebio, China) in the dark. After 14 days, the tissue blocks were removed and dehydrated in 15% sucrose solution at 4°C in the dark for 1 day, followed by dehydration in 30% sucrose solution for 2 days. After the tissue blocks were removed, they were washed with dd water for 1min, treated with concentrated ammonia water for 45min, and treated with fixing solution for 45min, and then dehydrated with 30% sucrose solution at 4°C in a dark environment for 3 days. Frozen sections were 100μm thick and finally sealed with glycerin gelatin and photographed.

QUANTIFICATION AND STATISTICAL ANALYSIS

Statistical analysis of the data were performed with GraphPad Prism (version 9.0) by a separate person who was unaware of the group assignments. At least three sample replicates were allocated for each group, and the results were expressed as standard error of the mean (SEM). Normality was assessed with the Shapiro-Wilk test. Differences between multiple groups were compared using one-way ANOVA, and a post-hoc test was applied to compare means among multiple groups. The Chi-square test was used for non-parametric data. The significance level was set as $P<0.05$.